Laboratory tests in borehole KFM01A, KFM08A, KFM11A, KFR102A and KFR104

Uniaxial compression and indirect tensile strength tests of intact rock

Caroline Hanquist, Lars Jacobsson, Sandra Davidsson
RISE Research Institutes of Sweden

This report concerns a study which was conducted for Svensk Kärnbränslehantering AB (SKB). The conclusions and viewpoints presented in the report are those of the author. SKB may draw modified conclusions, based on additional literature sources and/or expert opinions.

Data in SKB's database can be changed for different reasons. Minor changes in SKB's database will not necessarily result in a revised report. Data revisions may also be presented as supplements, available at www.skb.se.

This report is published on www.skb.se

SVENSK KÄRNBRÄNSLEHANTERING

Update notice

The original report, dated July 2023, was found to contain editorial errors which have been corrected in this updated version. The corrected factual errors are presented below.

Updated 2024-02

Location	Original text	Corrected text
Page 10, table 2-2, row 18	KFR104-110-18	KFR102A-110-18

Abstract

The density and mechanical properties were determined on water saturated specimens from boreholes KFM01A, KFM08A, KFM11A, KFR102A and KFR104 in the Forsmark site investigation area. The rock types in the selected sections were amphibolite (102017) and metavolcanic rock (103076). Some specimens had a more or less foliated rock structure. The cores were sampled from a depth ranging between 196–901 m.

The specimens were water saturated using tap water and all subsequent measurements were conducted at this moisture condition. The density was determined on 30 specimens. The testing ended with 20 indirect tensile tests yielding the indirect tensile strength and 10 uniaxial compression tests including the post-peak response yielded the Young's modulus, Poisson's ratio and the uniaxial compressive strength.

Some variation of rock material along the short cores could be seen, which is reflected in the measured data. The density at a water saturated condition was 2892–3067 kg/m^3 for amphibolite, and 2697–2763 kg/m^3 for metavolcanic rock.

The indirect tensile tests were conducted such that every specimen with visible foliation was tested with the diametrical compression across the foliation planes, with higher values for the indirect tensile strength on the specimens. The strength variation in the amphibolite was large. The indirect tensile strength was 10.8–21.4 MPa for amphibolite and 16.9–20.7 MPa for metavolcanic rock. Two of the amphibolite specimens had a deviating lower strength, indirect tensile strength 5.7 MPa respectively 5.8 MPa, with a ductile failure. Those specimens had a high content of mica.

The Young's modulus obtained from the uniaxial compression tests was 88.6–114.5 GPa for amphibolite and 68.2–89.1 GPa for metavolcanic rock and the Poisson's ratio was 0.339–0.386 for amphibolite and 0.236–0.313 for metavolcanic rock. The peak values of the axial compressive stress were in the range 213.1–333.7 MPa for amphibolite and 104.1–283.1 MPa for metavolcanic rock. One of the amphibolite specimens had a deviating lower strength and a ductile failure with Young's modulus 41.2 GPa, Poisson's ratio 0.500 and peak axial compressive stress of 44.5 MPa. That specimen had a high content of mica.

Sammanfattning

Densiteten och mekaniska egenskaper har bestämts på vattenmättade prover från borrhål KFM01A, KFM08A, KFM11A, KFR102A och KFR104 i Forsmarks platsundersökningsområde. Bergarterna i de valda avsnitten är amfibolit (102017) och vulkanit (103076). Några prover hade en mer eller mindre folierad bergstruktur. Proverna har tagits på djupnivåer mellan 196–901 m.

Proverna vattenmättades med kranvatten och alla efterföljande mätningar gjordes vid denna fukthalt. Densiteten mättes på samtliga 30 prover. Provningen avslutades med 20 stycken indirekta test av draghållfastheten som gav den indirekta draghållfastheten och 10 stycken enaxiella kompressions-försök inkluderat efterbrottsbeteende som gav värden på elasticitetsmodul, Poissons tal och enaxiell tryckhållfasthet.

En viss variation av bergmaterialet kunde ses på de korta kärnorna som visade sig i uppmätta data. Densiteten i ett vattenmättat tillstånd var 2892–3067 kg/m3 hos amfibolit och 2697–2763 kg/m3 hos vulkanit.

De indirekta dragförsöken utfördes så att alla prover med synlig foliationsriktning belastades med diametral kompression tvärs foliationsplanen. Styrkevariationen var stor hos amfibolit. Den indirekta draghållfastheten var 10,8–21,4 MPa hos amfibolit och 16,9–20,7 MPa hos vulkanit. Två av amfibolitproven hade en avvikande lägre hållfasthet, indirekt draghållfasthet 5,7 MPa respektive 5,8 MPa, med ett duktilt brottbeteende. Dessa prover hade en hög andel av glimmer.

Elasticitetsmodulen var 88,6–114,5 GPa hos amfibolit och 68,2–89,1 GPa hos vulkanit och Poissons tal var 0,339–0,386 hos amfibolit och 0,236–0,313 hos vulkanit. Toppvärdena för den kompressiva axiella spänningen låg mellan 213,1–333,7 MPa för amfibolit och 104,1–283,1 MPa för vulkanit. Ett av amfibolitproven hade en avvikande lägre hållfasthet och ett segt brottbeteende med elasticitetsmodul på 41,2 GPa, Poissons tal 0,500 och toppvärde för den kompressiva axiella spänningen på 44,5 MPa. Detta prov hade en hög andel av glimmer.

Content

1 Introduction

This document reports performance and results of measurements of density, indirect tensile tests and uniaxial compression tests, with loading beyond the failure point into the post-failure regime, on water-saturated drill core specimens. The drill cores originate from the boreholes KFM01A, KFM08A, KFM11A, KFR102A and KFR104 which are located within the site investigation area in Forsmark, see map in Figure 1-1. The boreholes are conventionally drilled cored boreholes, with a length of c 550–1000. The tests are concentrated to the rock types amphibolite (102017) and metavolcanic rock (103076).

The tests were carried out in the material and rock mechanics laboratories at the Department of Chemistry and Applied Mechanics and Department of Infrastructure and Concrete at RISE Research Institutes of Sweden in Borås.

SKB sent rock cores to RISE which arrived in Borås in October 2022 and were tested during November 2022 to January 2023. A planning of how to extract specimens was first conducted together with SKB. Cylindrical specimens were cut from the cores based on the plan. The end surfaces of the specimens were grinded in order to comply with the required shape tolerances. The specimens were water saturated and stored in water with a minimum of 7 days, up to testing. This yields a water saturation which is intended to resemble the in-situ moisture condition. All tests were carried out at this moisture condition. The density was first determined on each specimen followed by mechanical tests.

Figure 1-1. Geological map showing the location of boreholes drilled up to January 2023 within the Forsmark site. The projection of each borehole on the horizontal plane at top of casing is also shown in the figure. Cores from boreholes KFM01A, KFM08A, KFM11A, KFR102A and KFR104 are tested.

The method description SKB MD 160.002e was followed for the water saturation and density measurements. The method description SKB MD 190.004e was followed for the sampling and for the indirect tensile strength tests and the method description SKB MD 190.001e was followed for the uniaxial compression tests.

The controlling documents for the activity are listed in Table 1-1. Both Activity Plan and Method Descriptions are SKB's internal controlling documents, whereas the Quality Plan referred to in the table is a RISE internal controlling document.

Table 1-1 Controlling documents for performance of the activity.

Table head		
Activity plan	**Number**	**Version**
Laboratorieprovning hållfasthet amfibolit och vulkanit	AP SFK-22-032	1.0
Method descriptions	**Number**	**Version**
Determining density and porosity of intact rock	SKB MD 160.002e	3.0
Uniaxial compression test for intact rock	SKB MD 190.001e	4.0
Indirect test of tensile strength	SKB MD 190.004e	3.0
Quality plan		
Activity specific quality plan	RISE document	

2 Objective

The objective of this series of laboratory test is to increase the knowledge of amphibolite (SKB rock type code 102017) and the felsic to intermediate metavolcanic rock (103076), in the following denoted "metavolcanic rock"). Both these rock types are commonly occurring at the Forsmark site. The number of tests previously performed on samples from these rock types in Forsmark is limited. An increased number of laboratory strength test results will enable an improved description of the rock mechanical conditions of the site, which is required for the safety assessment of the planned final repository for spent nuclear fuel.

2.1 Extraction plan

A total of 26 core segments were selected for this investigation, four segments from KFM01A, eight segments from KFM08A, six segments from KFM11A, five segments from KFR102A and three segments from KFR104. A plan for how to extract specimens for the different investigations was made together with SKB. The markings of how to extract the specimens from the individual core segments including observations of defects are shown in Figures 2-1 to 2-2.

The rock type characterisation was made according to Stråhle (2001) using the SKB mapping system (Boremap). The labelling and position along the borehole (adjusted secup and adjusted seclow) and test designation for the individual specimens are shown in Table 2-1.

Figure 2-1. *Layout for cutting the uniaxial compression test specimens. The order of the specimens in the image follows, from top to bottom, Table 2-3.*

Figure 2-2. *Layout for cutting the indirect tensile test specimens. The order of the specimens in the image follows, from top to bottom, Table 2-2.*

Table 2-1. Core and specimen identification, sampling level (borehole length) and rock type for all specimens (based on the Boremap overview mapping).

Test specimen ID	Borehole	Adj Secup (m)	Adj Seclow (m)	Mechanical Test	Rock type/occurrence
110-01	KFM01A	260.22	260.25	BR	Amphibolite (102017)
110-02	KFM01A	260.25	260.28	BR	Amphibolite (102017)
113-01	KFM01A	260.38	260.51	UCS	Amphibolite (102017)
113-02	KFM01A	473.47	473.60	UCS	Amphibolite (102017)
110-03	KFM01A	473.86	473.89	BR	Amphibolite (102017)
110-04	KFM01A	473.89	473.92	BR	Amphibolite (102017)
113-03	KFM08A	556.48	556.61	UCS	Amphibolite (102017)
110-05	KFM08A	556.64	556.67	BR	Amphibolite (102017)
110-06	KFM08A	556.67	556.70	BR	Amphibolite (102017)
110-07	KFM08A	820.83	820.86	BR	Amphibolite (102017)
113-04	KFM08A	820.94	821.07	UCS	Amphibolite (102017)
110-08	KFM08A	821.42	821.45	BR	Amphibolite (102017)
110-09	KFM08A	900.94	900.97	BR	Amphibolite (102017)
113-05	KFM08A	900.99	901.12	UCS	Amphibolite (102017)
110-10	KFM08A	901.19	901.22	BR	Amphibolite (102017)
110-11	KFM11A	196.47	196.50	BR	Metavolcanic rock (103076)
110-12	KFM11A	196.77	196.80	BR	Metavolcanic rock (103076)
113-06	KFM11A	196.82	196.95	UCS	Metavolcanic rock (103076)
110-13	KFM11A	233.38	233.41	BR	Metavolcanic rock (103076)
113-07	KFM11A	233.44	233.57	UCS	Metavolcanic rock (103076)
110-14	KFM11A	233.64	233.67	BR	Metavolcanic rock (103076)
110-15	KFR102A	215.10	215.13	BR	Metavolcanic rock (103076)
113-08	KFR102A	215.16	215.29	UCS	Metavolcanic rock (103076)
110-16	KFR102A	215.33	215.36	BR	Metavolcanic rock (103076)
113-09	KFR102A	350.41	350.54	UCS	Metavolcanic rock (103076)
110-17	KFR102A	351.04	351.07	BR	Metavolcanic rock (103076)
110-18	KFR102A	351.07	351.10	BR	Metavolcanic rock (103076)
110-19	KFR104	420.26	420.29	BR	Metavolcanic rock (103076)
113-10	KFR104	426.26	426.39	UCS	Metavolcanic rock (103076)
110-20	KFR104	426.44	426.47	BR	Metavolcanic rock (103076)

Explanation to table: BR = Indirect tensile test (Brazilian), UCS = Uniaxial compression test.

2.2   Specimens for indirect tensile tests

A list of 20 specimens for the indirect tensile tests is shown in Table 2-2.

Table 2-2. Specimen identification, sampling level (borehole length) and rock type for all specimens (based on the Boremap overview mapping).

Identification	Adj Secup (m)	Adj Seclow (m)	Rock type/occurrence
KFM01A-110-01	260.22	260.25	Amphibolite (102017)
KFM01A-110-02	260.25	260.28	Amphibolite (102017)
KFM01A-110-03	473.86	473.89	Amphibolite (102017)
KFM01A-110-04	473.89	473.92	Amphibolite (102017)
KFM08A-110-05	556.64	556.67	Amphibolite (102017)
KFM08A-110-06	556.67	556.70	Amphibolite (102017)
KFM08A-110-07	820.83	820.86	Amphibolite (102017)
KFM08A-110-08	821.42	821.45	Amphibolite (102017)
KFM08A-110-09	900.94	900.97	Amphibolite (102017)
KFM08A-110-10	901.19	901.22	Amphibolite (102017)
KFM11A-110-11	196.47	196.50	Metavolcanic rock (103076)
KFM11A-110-12	196.77	196.80	Metavolcanic rock (103076)
KFM11A-110-13	233.38	233.41	Metavolcanic rock (103076)
KFM11A-110-14	233.64	233.67	Metavolcanic rock (103076)
KFR102A-110-15	215.10	215.13	Metavolcanic rock (103076)
KFR102A-110-16	215.33	215.36	Metavolcanic rock (103076)
KFR102A-110-17	351.04	351.07	Metavolcanic rock (103076)
KFR102A-110-18	351.07	351.10	Metavolcanic rock (103076)
KFR104-110-19	420.26	420.29	Metavolcanic rock (103076)
KFR104-110-20	426.44	426.47	Metavolcanic rock (103076)

2.3   Specimens for uniaxial compression tests

A list of 10 specimens for the uniaxial compression tests is shown in Table 2-3.

Table 2-3. Specimen identification, sampling level (borehole length) and rock type for all specimens (based on the Boremap overview mapping).

Identification	Adj Secup (m)	Adj Seclow (m)	Rock type/occurrence
KFM01A-113-01	260.38	260.51	Amphibolite (102017)
KFM01A-113-02	473.47	473.60	Amphibolite (102017)
KFM08A-113-03	556.48	556.61	Amphibolite (102017)
KFM08A-113-04	820.94	821.07	Amphibolite (102017)
KFM08A-113-05	900.99	901.12	Amphibolite (102017)
KFM11A-113-06	196.82	196.95	Metavolcanic rock (103076)
KFM11A-113-07	233.44	233.57	Metavolcanic rock (103076)
KFR102A-113-08	215.16	215.29	Metavolcanic rock (103076)
KFR102A-113-09	350.41	350.54	Metavolcanic rock (103076)
KFR104-113-10	426.26	426.39	Metavolcanic rock (103076)

3 Equipment

3.1 Specimen preparation and density measurement

A circular saw with a diamond blade was used to cut the specimens to their final lengths. The surfaces were then grinded after cutting in a grinding machine in order to achieve a high-quality surface for the axial loading that complies with the required tolerances. The measurements of the specimen dimensions were made with a sliding calliper. Furthermore, the tolerances were checked by means of a dial indicator and a stone face plate. The specimen preparation is carried out in accordance with ASTM (2001).

The following equipment was used for the density determinations:

- Scale for weight measurement after water saturation (scale routinely checked with reference weight). Measurement accuracy ± 0.002 g.

- Scale for weight measurement after water saturation in surface dry condition (scale routinely checked with reference weight). Measurement accuracy ± 0.02 g.

3.2 Indirect tensile strength test

The mechanical testing was carried out in a load frame where the crossbar is mechanically driven by screws and has a maximum load capacity of 100 kN in compression. The axial compressive load was measured by an external 100 kN load cell. The uncertainty of the load measurement is less than 1 %.

The frame was equipped with a pair of curved bearing blocks, radius 39 mm and width 29 mm, with pins for guiding the vertical deformation, see Figure 3-1. The top platen includes a spherical seating in order to have a fully centred loading position. The specimens were photographed with a digital camera and the photographs were stored in a jpeg-format.

Figure 3-1. Test-set up for the indirect tensile strength test. The load cell is visible in the top and the curved bearing blocks are seen below that.

3.3 Uniaxial compression test

The mechanical tests were carried out in a servo-controlled testing machine specially designed for rock tests, see Figure 3-2. The system consists of a load frame, a hydraulic pump unit, a controller unit and various sensors. The communication with the controller unit is accomplished by means of

special testing software run on a PC connected to the controller. The load frame is characterized by a high stiffness and is supplied with a fast responding actuator, cf. the ISRM suggested method (ISRM 1999).

Figure 3-2. *Rock testing system. From left: Digital controller unit, pressure cabinet (used for triaxial tests) and load frame. The PC with the test software (not shown in the picture) is placed on the left hand side of the controller unit.*

The stiffness of the various components of the loading chain in the load frame has been optimized in order to obtain a high total stiffness. This includes the load frame, load cell, load platens and piston, as well as having a minimum amount of hydraulic oil in the cylinder. Furthermore, the sensors, the controller and the servo valve are rapidly responding components. The axial load is determined using a load cell, which has a maximum capacity of 1.5 MN. The uncertainty of the load measurement is less than 1 %.

The axial and circumferential (radial) deformations of the rock specimens were measured. The rock deformation measurement systems are based on miniature LVDTs with a measurement range of ± 2.5 mm. The relative error for the LVDTs is less than 0.6 % within a 1 mm range for the axial deformation measurements and less than 1.3 % within a 3 mm range for the circumferential deformation measurement. The LVDTs have been calibrated by means of a micrometre.

Two independent systems were used for the axial deformation measurement in order to obtain two comparative results. The first system (S1), see Figure 3-3, comprises two aluminium rings attached on the specimen, placed at ¼ and ¾ of the specimen height. Two LVDTs mounted on the rings are used to measure the distance change between the rings on opposite sides of the specimen. As to the attachment, two rubber bands made of a thin rubber hose with a total thickness of 1 mm thickness are first mounted on the specimen right under where the two rings are to be positioned. The rings are supplied with three adjustable spring-loaded screws, each with a rounded tip pointing on the specimen with 120 degrees division. The screw tips are thus pressing on the rubber band, when the rings are mounted. The second system (S2), see Figure 3-3, consists of two aluminium plates clamped around the circular loading platens of steel on top and on bottom of the specimen. Two LVDTs, mounted on the plates, measure the distance change between these plates at opposite sides of the specimen at corresponding positions as for the first measurement system (S1).

The radial deformation was obtained by using a chain mounted around the specimen at mid-height, see Figure 3-3 and Appendix 1. The change of the chain-opening gap was measured by means of one LVDT and the circumferential, and thereby also the radial deformation could be obtained. See Appendix 1.

The specimens were photographed with a digital camera and the photographs were stored in a jpeg-format.
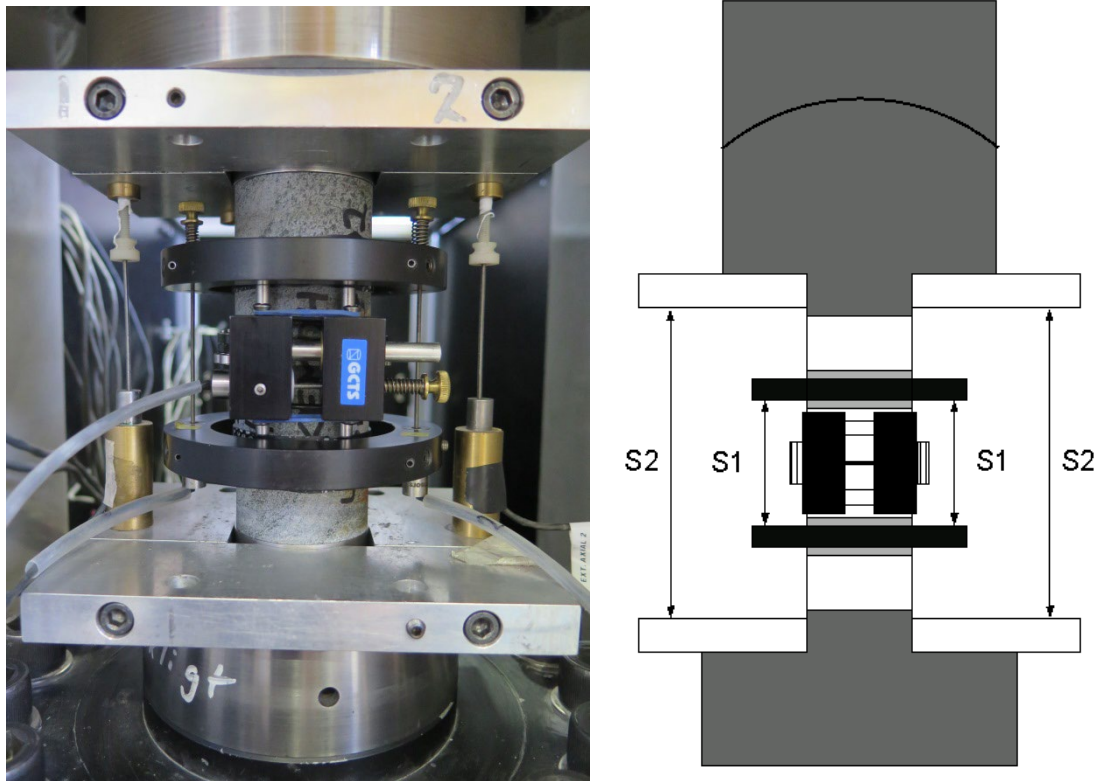
Figure 3-3. *Left: Specimen inserted between the loading platens. The two separate axial deformation measurement devices can be seen: system (S1) that measures the local axial deformation (rings), and system (S2) that measures the deformation between the aluminium plates (total deformation). Right: Principal sketch showing the two systems used for the axial deformation measurements.*

4 Execution

4.1 Specimen preparation

The steps for the specimen preparation are shown in Table 4-1.

Table 4-1. Activities during the specimen preparation.

Step	Activity
1	The drill cores were marked where the specimens are to be taken.
2	The specimens were cut to the specified length according to markings.
3	The cutting surfaces were grinded (only uniaxial compression test specimens)
4	The tolerances were checked: parallel and perpendicular end surfaces, smooth and straight circumferential surface.
5	The diameter and height were measured three times each. The respective mean value determines the dimensions that are reported.

4.2 Water saturation and density measurement

The water saturation and determination of the density of the wet specimens were made in accordance with the method description SKB MD 160.002e (SKB internal controlling document). This includes determination of density in accordance with ISRM (1979) and water saturation by EN 13755 (CEN 2008).

The specimens had been stored during 26 days in water when the density was determined. The density of the water at the time for the measurements was 998 kg/m^3. The execution procedure followed the prescription in SKB MD 160.002e, see Table 4-2.

Table 4-2. Activities during the water saturation and density measurements.

Step	Activity
1	The specimens were water saturated using tap water in normal air pressure for at least seven days.
2	The specimens were weighed in tap water. The temperature of the water was measured, and the water density was determined from a table.
3	The specimens were surface dried with a towel and weighed.
4	The density at a water saturated condition was determined.

4.3 Indirect tensile strength test

The specimens had been stored 28 days in water when the indirect tensile strength was determined.

An auto-calibration of the load frame was run prior to the mechanical test in order to check the system. Further, an individual checklist was filled in and checked for every specimen during all the steps in the execution.

The diameter and thickness were entered into the test software which computed the indirect tensile strength together with the mean value and standard deviation for the whole test series. The results were then exported as text-files and stored in a file server on the RISE computer network.

A list of the activities conducted during the indirect tensile strength tests is shown in Table 4-3.

Table 4-3. Activities during the indirect tensile strength tests.

Step	Activity
1	The direction of compressive loading was marked as a line on one of the plane surfaces with a marker pen.
2	Digital photos were taken on each specimen before the mechanical testing.
3	The wet specimens were inserted into the loading device one by one, with the correct orientation given by the marked line. The strain gauges were connected to the sampling device and the signals were checked. The specimens were loaded up to failure during deformation control. The displacement rate was set to 0.3 mm/min during loading. The maximum compressive load, which also defines the failure load, was registered.
4	Digital photos were taken on each specimen after the mechanical testing.

4.4 Uniaxial compression tests

4.4.1 Test procedure

The specimens had been stored 82-87 days in water when the uniaxial compression tests were carried out. The functionality of the testing system was checked before starting the tests.

An overview of the activities during the mechanical testing is shown in the step-by step description in Table 4-4.

Table 4-4. Activities during the uniaxial compression tests.

Step	Activity
1	Digital photos were taken on each specimen before the mechanical testing.
2	Devices for measuring axial and circumferential deformations were attached to the specimen.
3	The specimen was put in place and centred between the frame loading platens.
4	The core on each LVDT was adjusted by means of a set screw to the right initial position. This was done so that the optimal range of the LVDTs can be used for the deformation measurement.
5	The frame piston was brought down into contact with the specimen with a force corresponding to 1.0 MPa axial stress.
6	A load cycle with loading up to 5 MPa and unloading to 1.0 MPa was conducted in order to settle possible contact gaps in the spherical seat in the piston and between the rock specimen and the loading platens.
7	The centring was checked again.
8	The deformation measurement channels were zeroed in the test software.
9	The loading was started and the initial loading rate was set to a radial strain rate of -0.025 %/min. The loading rate was increased after reaching the post-failure region. This was done in order to prevent the total time for the test to become too long.
10	The test was stopped either manually when the test had proceeded long enough to reveal the post-failure behaviour, or after severe cracking had occurred and it was judged that very little residual axial loading capacity was left in the specimen.
11	Digital photos were taken on each specimen after the mechanical testing.

4.4.2 Analyses and interpretation

As to the definition of the different results parameters we begin with the axial stress σ_a, which is defined as

$$\sigma_a = \frac{F}{A}$$

where F is the axial force acting on the specimen, and A is the specimen cross section area. The peak value of the axial stress during a test is representing the uniaxial compressive strength σ_c in the results presentation.

The average value of the two axial displacement measurements on opposite sides of the specimen is used for the axial strain calculation, cf. Figure 4-5. In the first measurement system (S1), the recorded deformation represents a local axial deformation δ_{local} between the points at ¼ and ¾ height. A local axial strain is defined as

$$\varepsilon_{a,local} = \delta_{local}/L_{local}$$

where L_{local} is the centre to centre distance between the rings before loading.

In the second measurement system (S2), the recorded displacement corresponds to a total deformation that, in addition to total rock deformation, also contains the local deformations that occur in the contact between the rock and the loading platens, and further it also contains the deformation of the steel loading platens at each side of the specimen ends. The average value of the two total deformation measurements on opposite sides of the specimen is defined as the total deformation δ_{total}. An axial strain based on the total of the deformation is defined as

$$\varepsilon_{a,total} = \delta_{total}/L_{total}$$

where L_{total} is the height of the rock specimen.

The radial deformation is measured by means of a chain mounted around the specimen at mid-height, cf. Figure 3-3. The change of chain opening gap is measured by means of one LVDT. This measurement is used to compute the radial strain ε_r, see Appendix 1. Moreover, the volumetric strain ε_{vol} is defined as

$$\varepsilon_{vol} = \varepsilon_a + 2\varepsilon_r$$

The stresses and the strains are defined as positive in compressive loading and deformation. The elasticity parameters are defined by the tangent Young's modulus E and tangent Poisson's ratio ν as

$$E = \frac{\sigma_a(0.60\sigma_c) - \sigma_a(0.40\sigma_c)}{\varepsilon_a(0.60\sigma_c) - \varepsilon_a(0.40\sigma_c)}$$

$$\nu = -\frac{\varepsilon_r(0.60\sigma_c) - \varepsilon_r(0.40\sigma_c)}{\varepsilon_a(0.60\sigma_c) - \varepsilon_a(0.40\sigma_c)}$$

The tangents were evaluated with values corresponding to an axial load between 40 % and 60 % of the axial peak stress σ_c.

Two important observations can be made from the results:

i. The results based on the total axial deformation measurement (S2) display a lower axial stiffness, i.e., a lower value on Young's modulus, than in the case when the results are based on the local axial deformation measurement (S1). This is due to the additional deformations from the contact interface between the rock specimen and the steel loading platens and also due to the deformation of the loading platens themselves.

ii.   It can be seen that the response differs qualitatively between the results obtained with the local axial deformation measurement system (S1) and the system that measures total axial deformation (S2). In some cases, the post-peak response obtained with the local deformation measurement system seems not to be physically correct. This can be due to a number of reasons, e.g., that a crack caused a localized deformation, see Figure 4-1. Another explanation could be that the rings attached to the specimens have slightly slipped or moved, for example if a crack was formed nearby one of the attachment points.

It is reasonable to assume that results based on the local axial deformation measurement (S1) are fairly accurate up to the formation of the first macro-cracks or up to the peak load, but not thereafter. However, the results obtained with the total axial deformation measurement (S2) seem to be qualitatively correct after failure. We will therefore report the results based on the total axial deformation measurement, but carry out a correction of those results as described below in order to obtain overall good results.

The total axial deformation δ_{total} measured by (S2) is a summation of several deformations

$$\delta_{total} = \delta_{rock} + \delta_{system} \qquad (1)$$

where

$$\delta_{system} = \delta_{interface} + \delta_{loading\ platens}$$

and δ_{rock} is the axial deformation of the whole rock specimen. Assume that the system deformation is proportional to the applied axial force F in the loading chain, i.e.

$$\delta_{system} = F/K_{system} \qquad (2)$$

where K_{system} is the axial stiffness in the system (containing the interface between the rock and loading platens and the deformation of the loading platens). Combining (1) and (2) leads to

$$\delta_{rock} = \delta_{total} - F/K_{system} \qquad (3)$$

where an expression of the axial deformation in the whole specimen is obtained. This can be viewed as a correction of the measurements made by system (S2). By using δ_{rock} to represent the axial deformation of the specimen that is based on a correction of the results of the total axial deformation will yield good results both in the loading range up to failure and at loading after failure. However, it is noticed that K_{system} is not known and has to be determined.
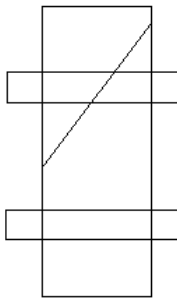
Figure 4-1. Example of cracking that may cause results that are difficult to interpret with a local deformation measurement.

It was previously suggested that the local axial deformation measurement (S1) represents the real rock deformation well up to the load where the macro-cracks form. Further, it is fair to assume that the axial deformation is homogenous at this part of the loading. Hence, we get

$$\delta_{rock} = \delta_{local} \cdot L_{total}/L_{local} \qquad (4)$$

This yields representative values of the total rock deformation for the first part of the loading up to the point where macro-cracking is taking place. It is now possible to determine δ_{system} up to the threshold of macro-cracking by combining (1) and (4) which yields

$$\delta_{\text{system}} = \delta_{\text{total}} - \delta_{\text{local}} \cdot L_{\text{total}}/L_{\text{local}} \qquad (5)$$

Finally, we need to compute K_{system}. By rewriting (2) we get

$$K_{\text{system}} = \frac{F}{\delta_{\text{system}}}$$

We will compute the system stiffness based on the results between 40 % and 60 % of the axial peak stress σ_{c}. This means that the Young's modulus and the Poisson's ratio will take the same values both when the data from the local axial deformation measurement (S1) and when the data from corrected total axial deformation are used. Thus, we have

$$K_{\text{system}} = \frac{F(0.60\sigma_{\text{c}}) - F(0.40\sigma_{\text{c}})}{\delta_{\text{system}}(0.60\sigma_{\text{c}}) - \delta_{\text{system}}(0.40\sigma_{\text{c}})} \qquad (6)$$

The results based on the correction according to (3) and (6) are presented in Section 6.4, whereas the original measured unprocessed data are reported in Appendix 2.

A closure of present micro-cracks will take place initially during axial loading. Development of new micro-cracks will start when the load is further increased and axial stress reaches the crack initiation stress σ_{i}. The crack growth at this stage is as stable as increased loading is required for further cracking. A transition from a development of micro-cracks to macro-cracks will occur when the axial load is further increased. At a certain stress level, the crack growth becomes unstable. The stress level when this happens is denoted the crack damage stress σ_{d}, cf. Martin and Chandler (1994). In order to determine the stress levels, we look at the volumetric strain.

By subtracting the elastic volumetric strain $\varepsilon_{\text{vol}}^{\text{e}}$ from the total volumetric strain, a volumetric strain corresponding to the crack volume $\varepsilon_{\text{vol}}^{\text{cr}}$ is obtained. This has been denoted calculated crack volumetric strain in the literature, cf. Martin and Chandler (1994) and Eberhardt et al. (1998). We thus have

$$\varepsilon_{\text{vol}}^{\text{cr}} = \varepsilon_{\text{vol}} - \varepsilon_{\text{vol}}^{\text{e}}$$

Assuming linear elasticity leads to

$$\varepsilon_{\text{vol}}^{\text{cr}} = \varepsilon_{\text{vol}} - \frac{1 - 2\upsilon}{E}\sigma_{\text{a}}$$

where $\sigma_{\text{r}} = 0$ was used. Experimental investigations have shown that the crack initiation stress σ_{i} coincides with the onset of increase of the calculated crack volume, cf. Martin and Chandler (1994) and Eberhardt et al. (1998). The same investigations also indicate that the crack damage stress σ_{d} can be defined as the axial stress at which the total volume starts to increase, i.e. when a dilatant behaviour is observed.

Another method to assess the crack initiation stress based on strain measurements is to use the Inverse Tangent Lateral Stiffness, cf. Ghazvinian et al. (2012), which was used in e.g. Jacobsson et al. (2016).

4.5   Data handling

The test results were transferred to and stored in a file server on the RISE computer network after completed tests. The main data processing, in which the elastic moduli were computed and the peak stress was determined, has been carried out using the program MATLAB, MathWorks (2021). Moreover, MATLAB was used to produce the diagrams shown in Section 5.3 and in Appendix 2. MS Excel was used to produce the other diagrams and for reporting data to the SICADA database.

4.6   Nonconformities

The testing was conducted according to the method description with some deviations. The circumferential strains have been determined within a relative error of 1.5 %, which is larger than what is specified in the ISRM-standard (ISRM 1999). Further, double systems for measuring the axial deformation have been used, which is beyond the specifications in the method description. This was conducted as development of the test method specially aimed for high-strength brittle rock.

The activity plan was followed with no departures.

Two uniaxial compression test specimens had a deviation from straightness of 0.35 mm (KFM08A-113-03) and 0.45 mm (KFM08A-113-04) which are larger than the limit of 0.3 mm given in ISRM (1999).

5 Results

The reported parameters are based both on unprocessed raw data obtained from the testing and processed data and were reported to the Sicada database, where they are traceable by the activity plan number. These data together with the digital photographs of the individual specimens were handed over to SKB. The handling of the results follows SDP-508 (SKB internal controlling document) in general.

5.1 Density

The density of the specimens at a water saturated condition is shown in the results tables for the mechanical tests in Sections 5.2 and 5.3. An overview of the results for all specimens is shown in Figure 5-1.
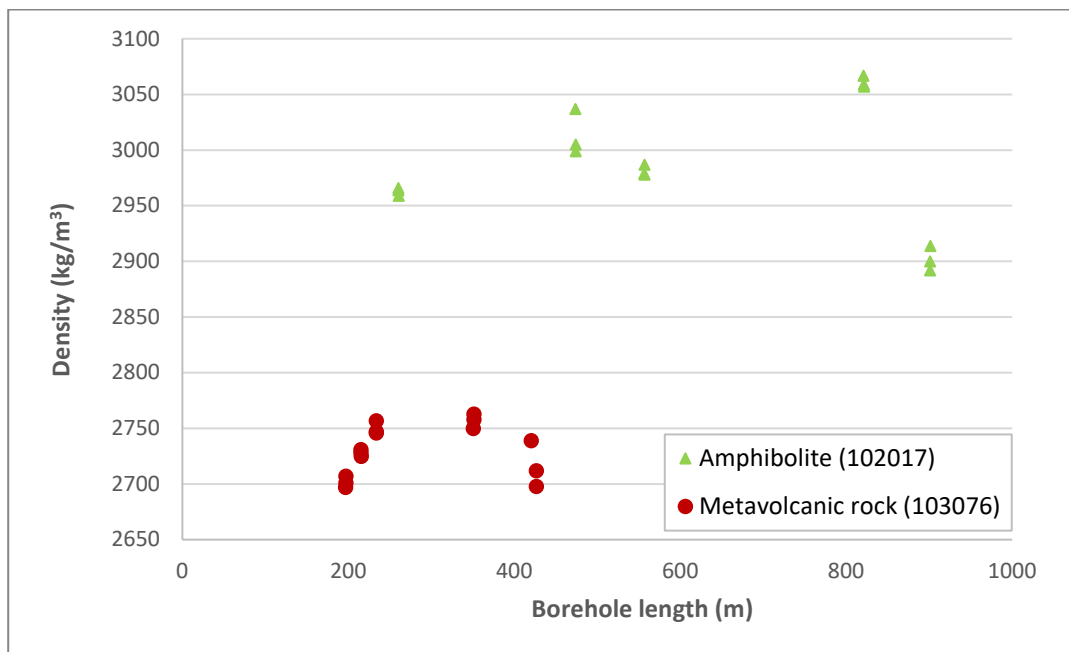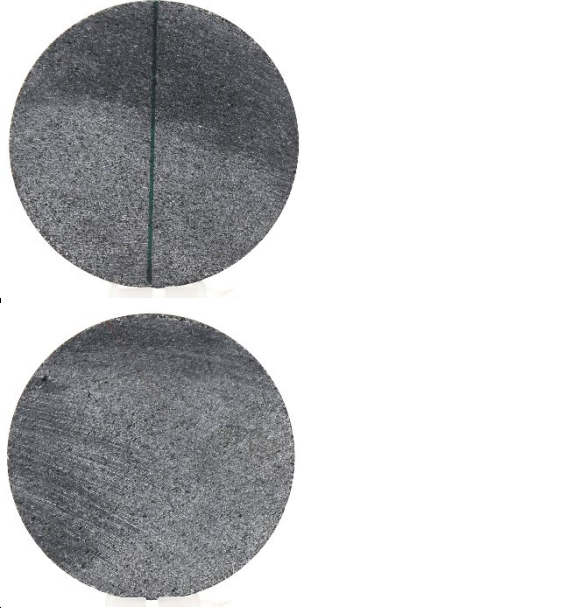
Figure 5-1. Density as a function of the borehole length for the two rock types in the study.
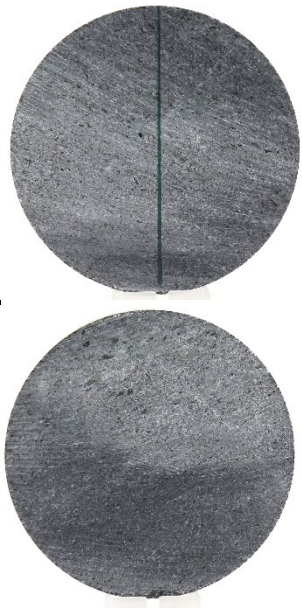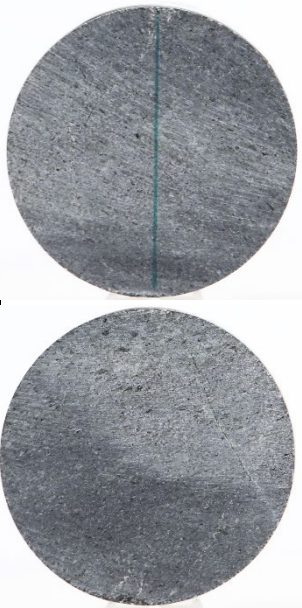
5.2 Indirect tensile strength test
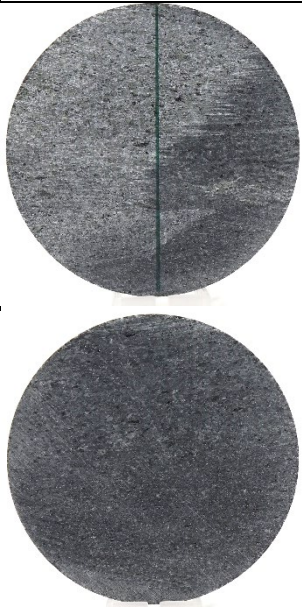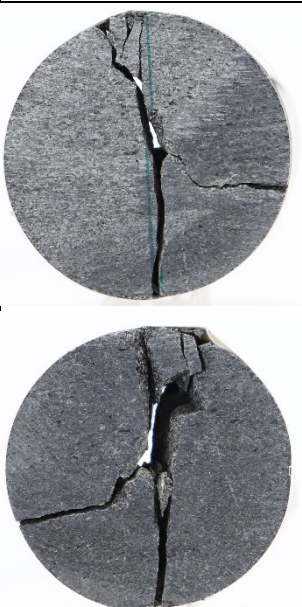
5.2.1 Results for each individual specimen

The results and photographs for the individual specimen are presented below.
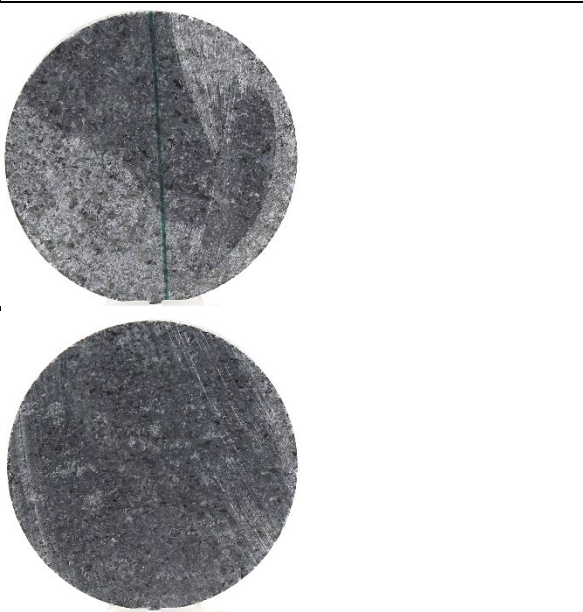
Specimen ID: KFM01A-110-01	
Before mechanical test	After mechanical test

Diameter (mm)	Height (mm)	Density (kg/m³)	Tensile strength (MPa)
50.8	26.4	2964	10.7
Comments:	None		

Specimen ID: KFM01A-110-02	
Before mechanical test	After mechanical test

Diameter (mm)	Height (mm)	Density (kg/m³)	Tensile strength (MPa)
50.8	25.7	2966	15.2
Comments:	None		

Specimen ID: KFM01A-110-03	
Before mechanical test	After mechanical test

Diameter (mm)	Height (mm)	Density (kg/m³)	Tensile strength (MPa)
50.7	25.8	2999	20.1
Comments:	None		

Specimen ID: KFM01A-110-04	
Before mechanical test	After mechanical test

Diameter (mm)	Height (mm)	Density (kg/m³)	Tensile strength (MPa)
50.7	26.5	3005	18.6
Comments:	None		
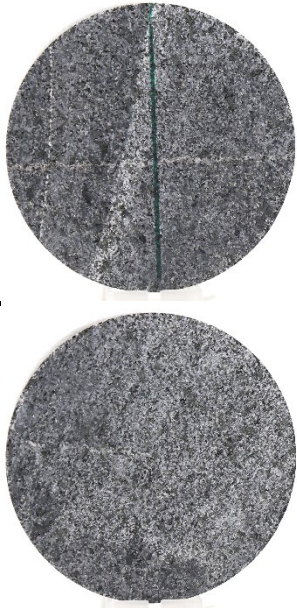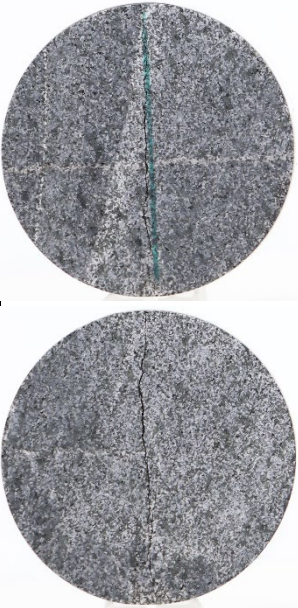
Specimen ID: KFM08A-110-05	
Before mechanical test	After mechanical test

Diameter (mm)	Height (mm)	Density (kg/m³)	Tensile strength (MPa)
50.3	26.4	2987	18.8
Comments:	None		
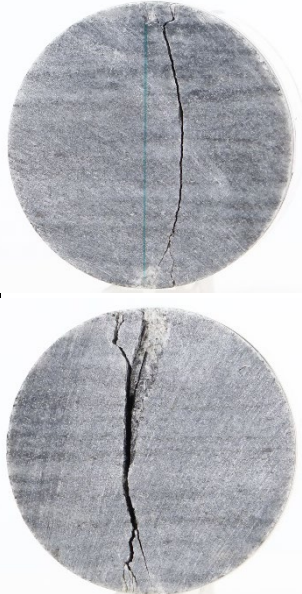
Specimen ID: KFM08A-110-06	
Before mechanical test	After mechanical test

Diameter (mm)	Height (mm)	Density (kg/m³)	Tensile strength (MPa)
50.3	26.3	2978	21.4
Comments:	None		
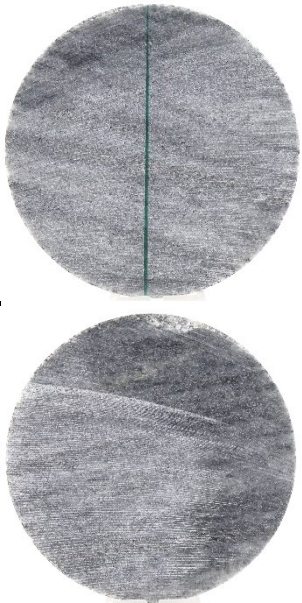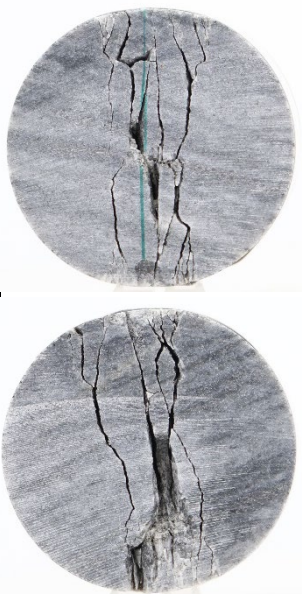
Specimen ID: KFM08A-110-07	
Before mechanical test	After mechanical test

Diameter (mm)	Height (mm)	Density (kg/m³)	Tensile strength (MPa)
50.6	25.9	3067	5.68
Comments:	There was a ductile failure. See comment below on KFM08A-113-04.		
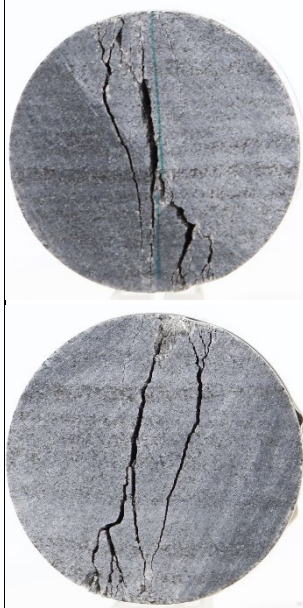
Specimen ID: KFM08A-110-08	
Before mechanical test	After mechanical test

Diameter (mm)	Height (mm)	Density (kg/m³)	Tensile strength (MPa)
50.6	26.4	3057	5.80
Comments:	There was a ductile failure. See comment below on KFM08A-113-04.		
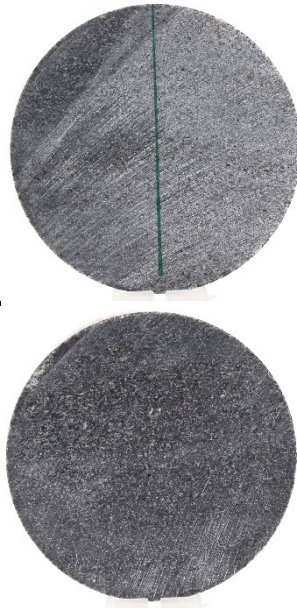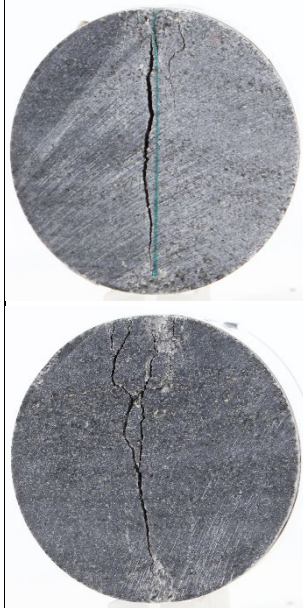
Specimen ID: KFM08A-110-09	
Before mechanical test	After mechanical test

Diameter (mm)	Height (mm)	Density (kg/m³)	Tensile strength (MPa)
50.5	26.8	2892	16.4
Comments:	None		

Specimen ID: KFM08A-110-10	
Before mechanical test	After mechanical test

Diameter (mm)	Height (mm)	Density (kg/m³)	Tensile strength (MPa)
50.5	26.0	2914	12.1
Comments:	None		
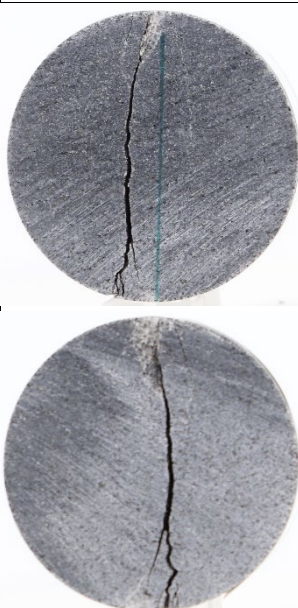
Specimen ID: KFM11A-110-11	
Before mechanical test	After mechanical test

Diameter (mm)	Height (mm)	Density (kg/m³)	Tensile strength (MPa)
50.9	26.0	2697	20.6
Comments:	None		

Specimen ID: KFM11A-110-12	
Before mechanical test	After mechanical test

Diameter (mm)	Height (mm)	Density (kg/m³)	Tensile strength (MPa)
50.9	25.7	2707	20.7
Comments:	None		

Specimen ID: KFM11A-110-13	
Before mechanical test	After mechanical test

Diameter (mm)	Height (mm)	Density (kg/m³)	Tensile strength (MPa)
50.8	26.5	2747	18.1
Comments:	None		

Specimen ID: KFM11A-110-14	
Before mechanical test	After mechanical test

Diameter (mm)	Height (mm)	Density (kg/m³)	Tensile strength (MPa)
50.8	26.8	2746	17.0
Comments:	None		
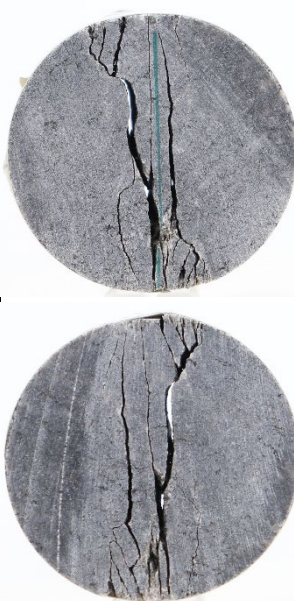
Specimen ID: KFR102A-110-15	
Before mechanical test	After mechanical test

Diameter (mm)	Height (mm)	Density (kg/m^3)	Tensile strength (MPa)
50.2	26.1	2728	19.8
Comments:	None		

Specimen ID: KFR102A-110-16	
Before mechanical test	After mechanical test

Diameter (mm)	Height (mm)	Density (kg/m^3)	Tensile strength (MPa)
50.2	26.0	2725	19.3
Comments:	None		

Specimen ID: KFR102A-110-17	
Before mechanical test	After mechanical test

Diameter (mm)	Height (mm)	Density (kg/m³)	Tensile strength (MPa)
50.2	25.8	2763	16.9
Comments:	None		

Specimen ID: KFR104-110-18	
Before mechanical test	After mechanical test

Diameter (mm)	Height (mm)	Density (kg/m³)	Tensile strength (MPa)
50.2	25.9	2758	19.2
Comments:	None		

Specimen ID: KFR104-110-19

Before mechanical test	After mechanical test

Diameter (mm)	Height (mm)	Density (kg/m³)	Tensile strength (MPa)
50.0	26.1	2739	18.8
Comments:	None		

Specimen ID: KFR104-110-20

Before mechanical test	After mechanical test

Diameter (mm)	Height (mm)	Density (kg/m³)	Tensile strength (MPa)
50.0	24.2	2698	17.9
Comments:	None		

5.2.2 Results for the entire test series

The test results are shown in Table 5-1 and Figure 5-2.

Table 5-1. Results from density measurements and direct tensile tests.

Identification	Density (kg/m^3)	Tensile strength (MPa)	Comments
KFM01A-110-01	2964	10.7	I (I = Isotropic)
KFM01A-110-02	2966	15.2	I
KFM01A-110-03	2999	20.1	I
KFM01A-110-04	3005	18.6	I
KFM08A-110-05	2987	18.8	I
KFM08A-110-06	2978	21.4	I
KFM08A-110-07	3067	5.68	I
KFM08A-110-08	3057	5.80	I
KFM08A-110-09	2892	16.4	I
KFM08A-110-10	2914	12.1	I
KFM11A-110-11	2697	20.6	PF (PF = load line perpendicular to foliation)
KFM11A-110-12	2707	20.7	PF
KFM11A-110-13	2747	18.1	PF
KFM11A-110-14	2746	17.0	I
KFR102A-110-15	2728	19.8	I
KFR102A-110-16	2725	19.3	I
KFR102A-110-17	2763	16.9	I
KFR104-110-18	2758	19.2	I
KFR104-110-19	2739	18.8	I
KFR104-110-20	2698	17.9	I
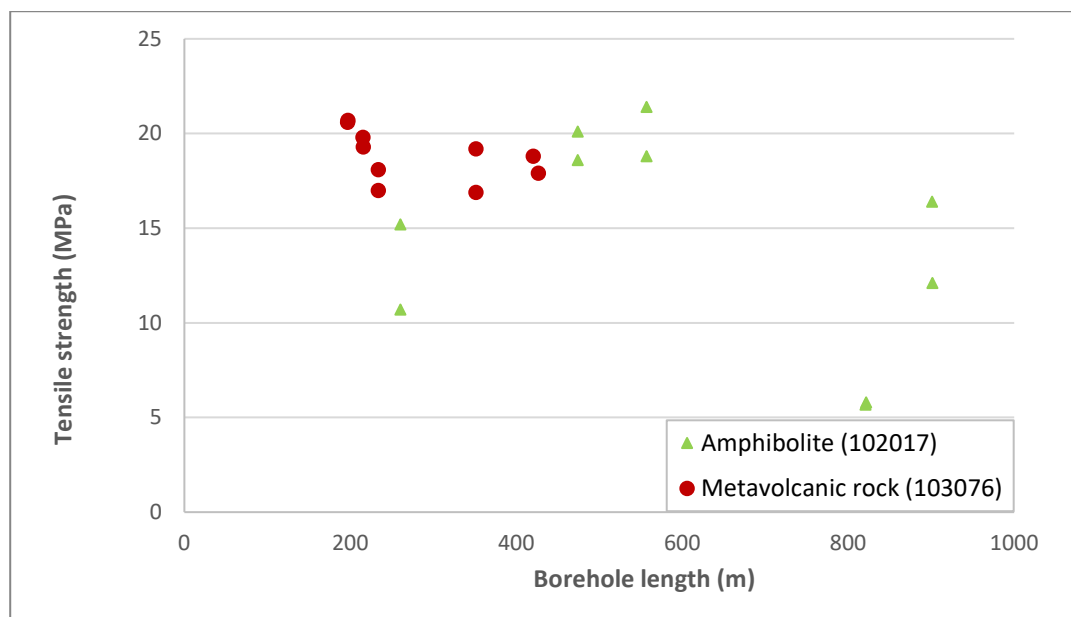
Figure 5-2. *Indirect tensile strength as a function of the borehole length for the two rock types.*

5.3 Uniaxial compression test

5.3.1 Results for each individual specimen

The cracking is shown in photos of the specimens, and comments on observations made during the testing are reported. The elasticity parameters have been evaluated by using the results from the local axial deformation measurements. The data from the adjusted total axial deformation measurements, cf. Section 4.4.2, are shown in this section.

Diagrams showing the data from both the local and the total axial deformation measurements, system (S1) and (S2) in Figure 3-3, and the computed individual values of K_{system} used at the data corrections are shown in Appendix 2. Diagrams displaying actual radial strain rates versus the test time are also presented in Appendix 2. The results for the individual specimens are as follows:

Specimen ID: KFM01A-113-01	
Before mechanical test	After mechanical test

Diameter (mm)	Height (mm)	Density (kg/m³)	
50.8	127.8	2959	

Comments:
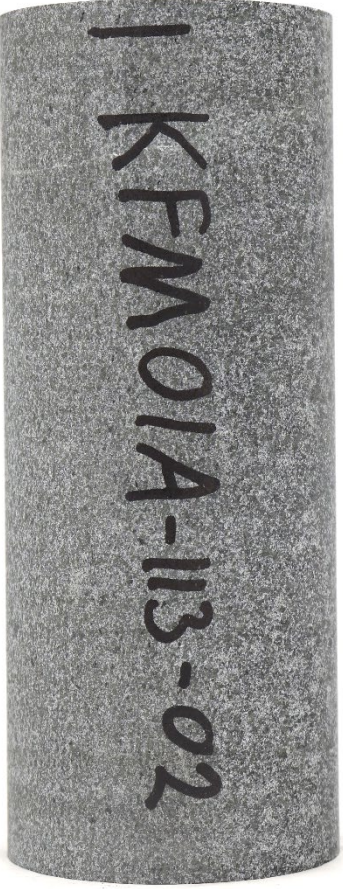
Specimen ID: KFM01A-113-01

Youngs Modulus (E):	88.6	[GPa]
Poisson Ratio (ν):	0.386	[-]
Axial peak stress (σ_c):	213.1	[MPa]
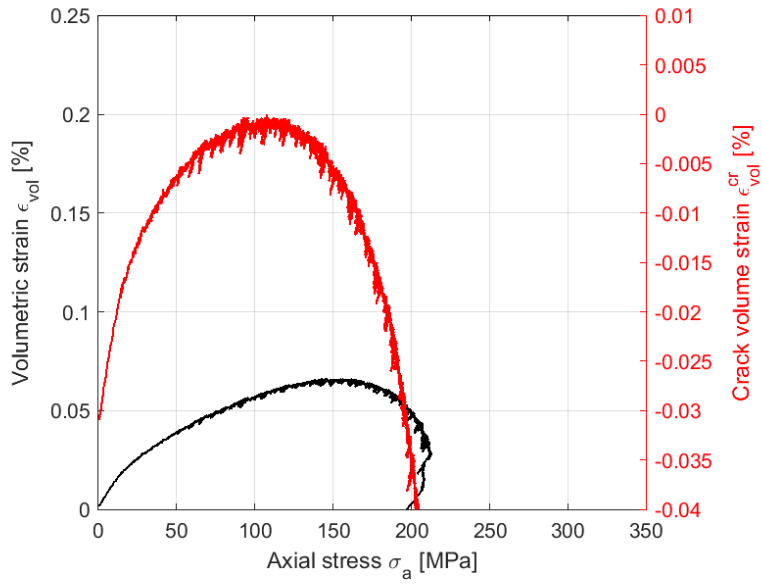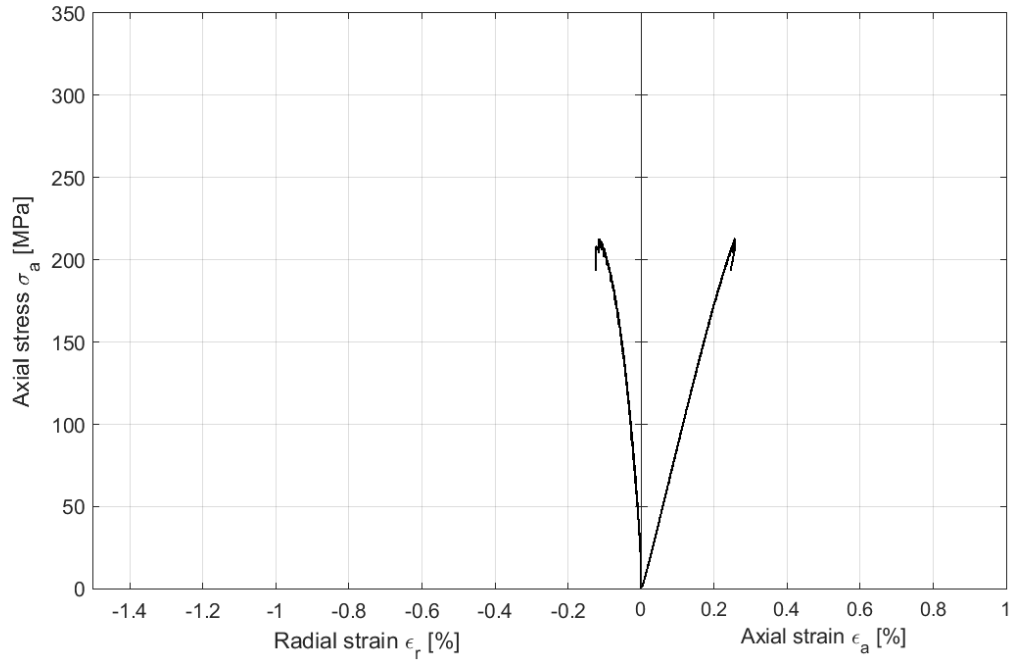
Specimen ID: KFM01A-113-02			
Before mechanical test	After mechanical test		
Diameter (mm)	Height (mm)	Density (kg/m³)	
50.7	126.7	3037	
Comments:			

Specimen ID: KFM01A-113-02

Youngs Modulus (E):	114.5	[GPa]
Poisson Ratio (ν):	0.345	[-]
Axial peak stress (σ_c):	333.7	[MPa]

Specimen ID: KFM08A-113-03	
Before mechanical test	After mechanical test

Diameter (mm)	Height (mm)	Density (kg/m³)	
50.3	127.7	2979	
Comments:	The specimen had a deviation from straightness of 0.35 mm.		
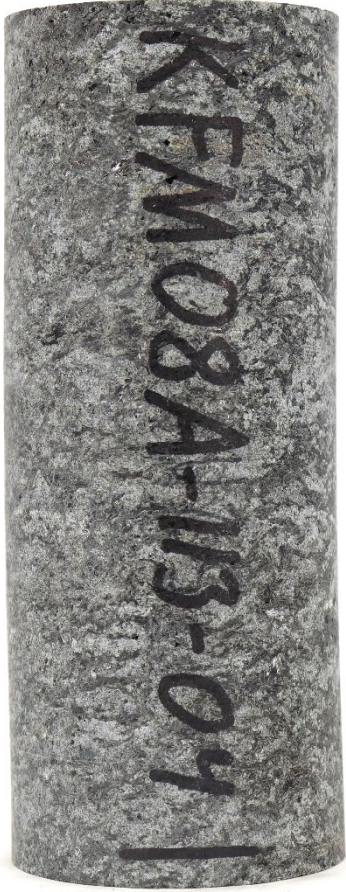
Specimen ID: KFM08A-113-03

Youngs Modulus (E):	101.4	[GPa]
Poisson Ratio (ν):	0.339	[-]
Axial peak stress (σ_c):	289.2	[MPa]

Specimen ID: KFM08A-113-04	
Before mechanical test	After mechanical test

Diameter (mm)	Height (mm)	Density (kg/m³)	
50.6	126.7	3059	

Comments:	The specimen had a deviation from straightness of 0.45 mm. The observed ductile response and low strength has been judged to be due to a high content of mica in the specimen (approximately 30-40 %). Moreover, bands of mica concentrations are seen throughout the specimen. In addition, green minerals can be seen. They were a silicate mineral belonging to the pyroxene group, e.g. diopside/hedenbergite. This was verified by an micro XRF analysis (chemical content). The occurrence of pyroxenes may contribure to the observed ductile and weaker behavior.

Specimen ID: KFM08A-113-04

Youngs Modulus (E):	41.2	[GPa]
Poisson Ratio (ν):	0.500	[-]
Axial peak stress (σ_c):	44.5	[MPa]
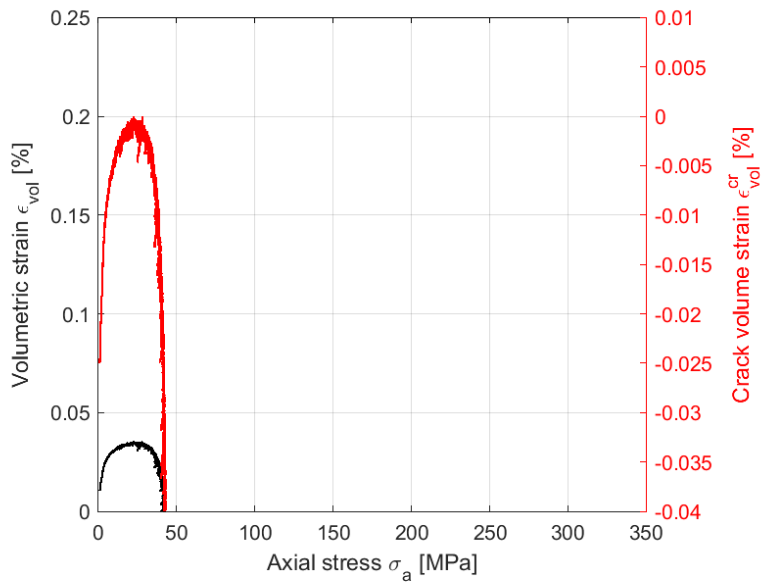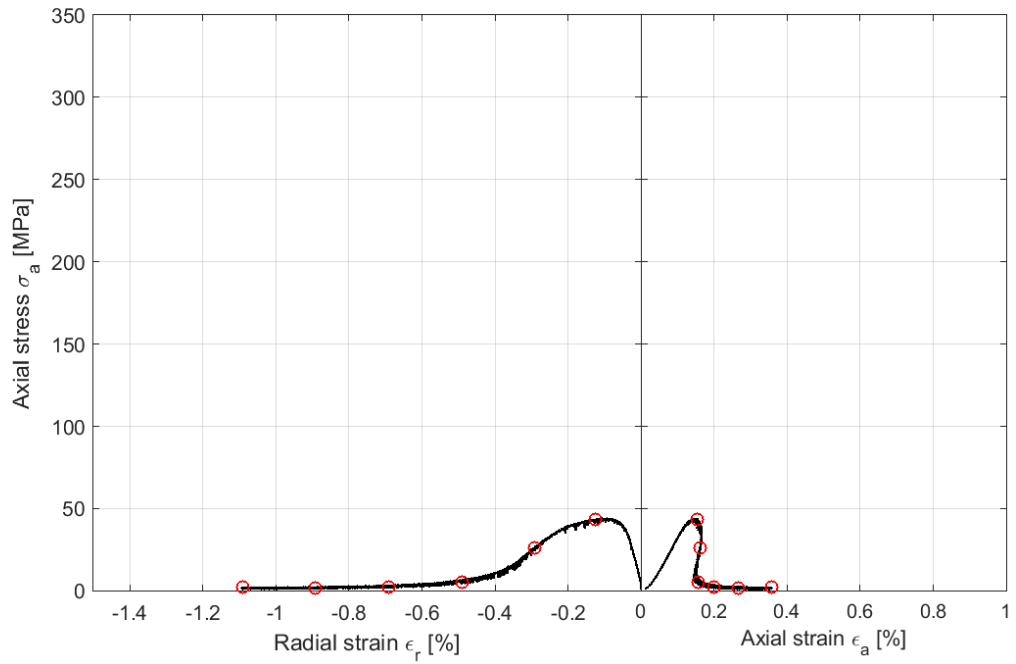
Specimen ID: KFM08A-113-05			
Before mechanical test	After mechanical test		
Diameter (mm)	**Height (mm)**	**Density (kg/m³)**	
50.5	127.7	2900	
Comments:	Inclined 0.5 mm		
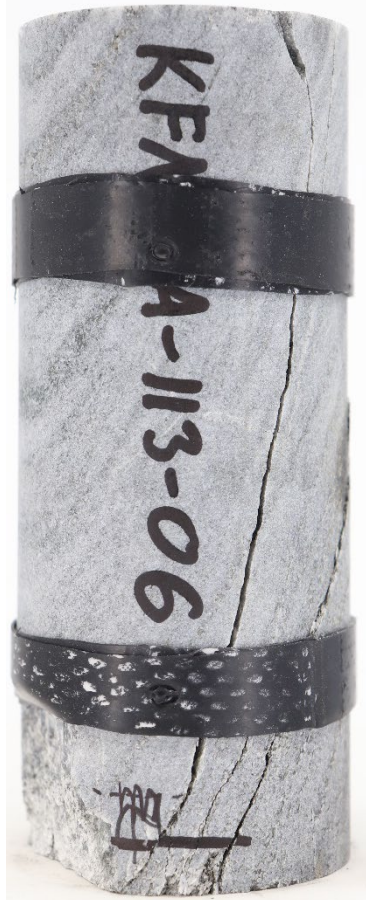
Specimen ID: KFM08A-113-05

Youngs Modulus (E):	89.3	[GPa]
Poisson Ratio (ν):	0.384	[-]
Axial peak stress (σ_c):	252.8	[MPa]
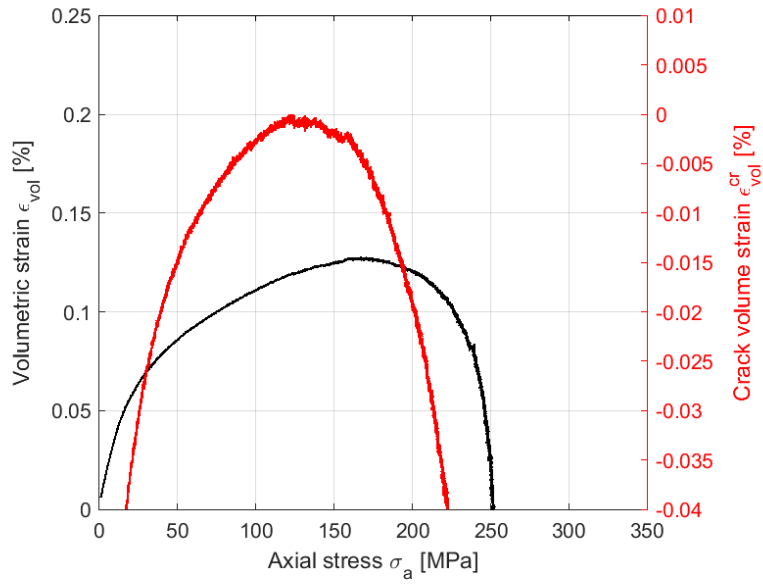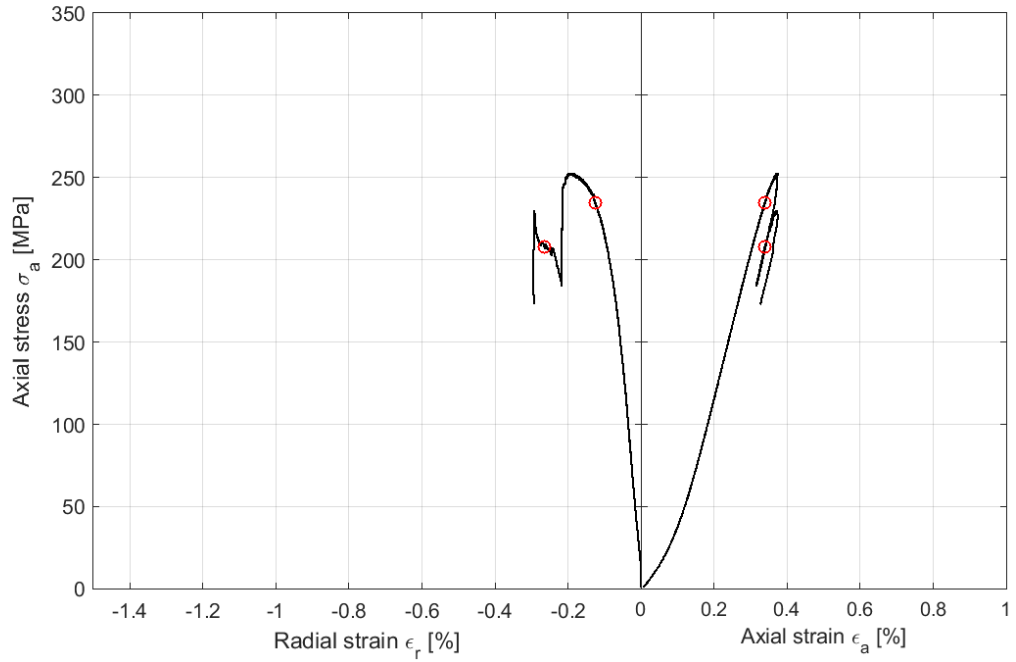
Specimen ID: KFM11A-113-06			
Before mechanical test	After mechanical test		
Diameter (mm)	Height (mm)	Density (kg/m³)	
50.9	128.8	2701	
Comments:			
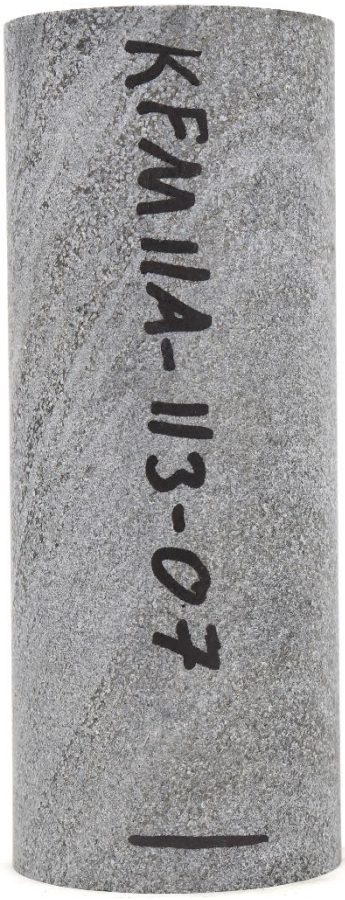
Specimen ID: KFM11A-113-06

Youngs Modulus (E):	88.8	[GPa]
Poisson Ratio (ν):	0.236	[-]
Axial peak stress (σ_c):	132.4	[MPa]
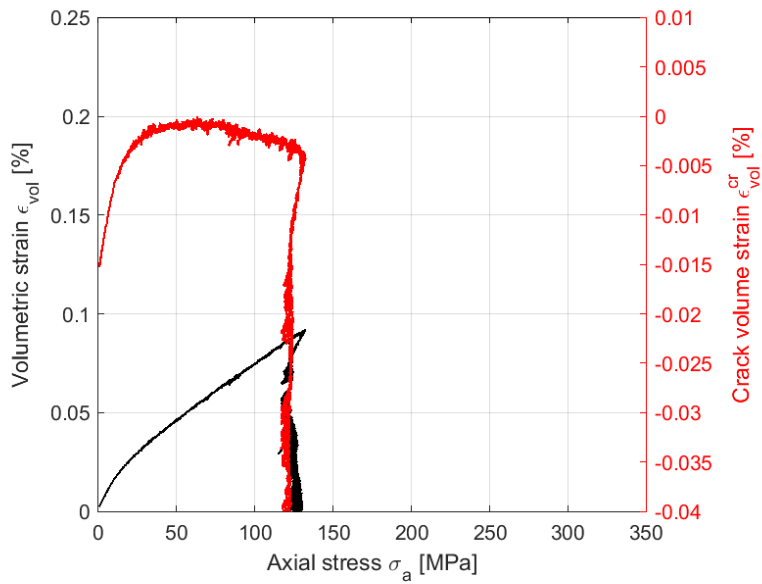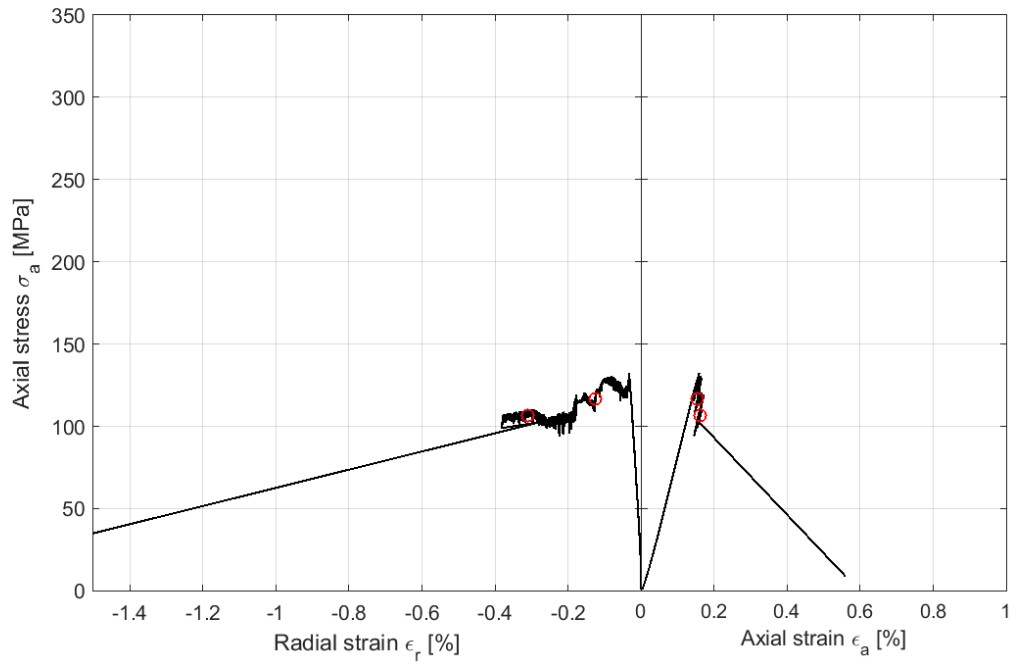
Specimen ID: KFM11A-113-07			
Before mechanical test	After mechanical test		
Diameter (mm)	Height (mm)	Density (kg/m³)	
50.8	128.9	2757	
Comments:			
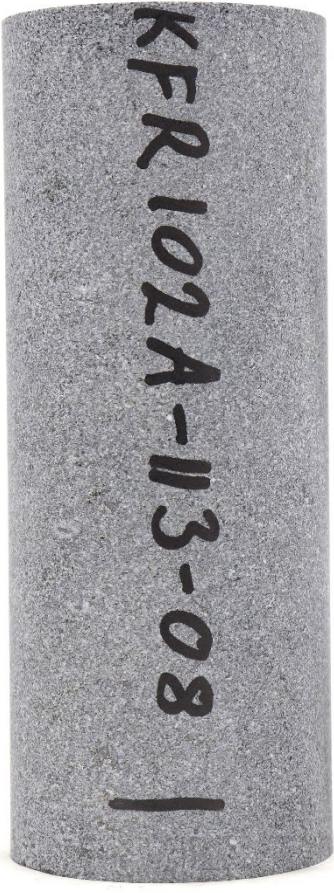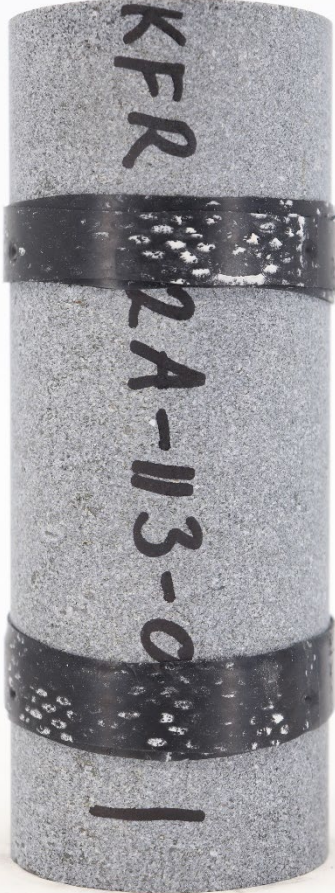
Specimen ID: KFM11A-113-07

Youngs Modulus (E):	77.3	[GPa]
Poisson Ratio (ν):	0.326	[-]
Axial peak stress (σ_c):	122.2	[MPa]
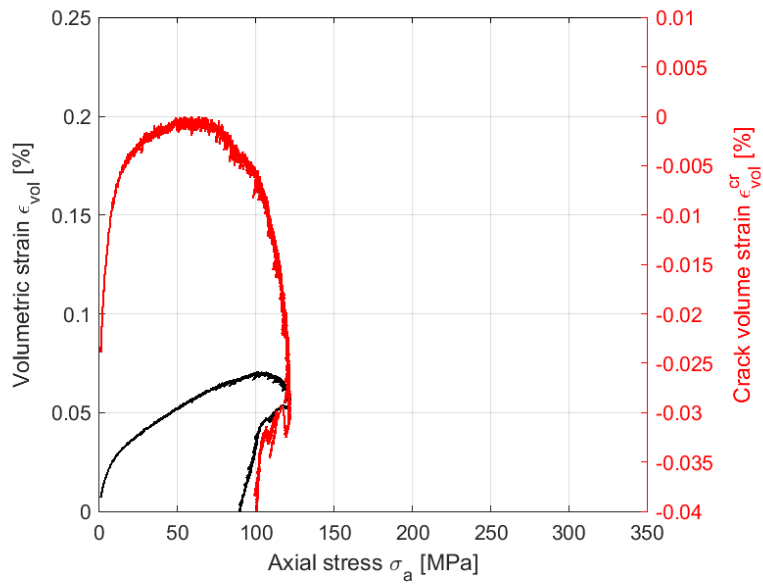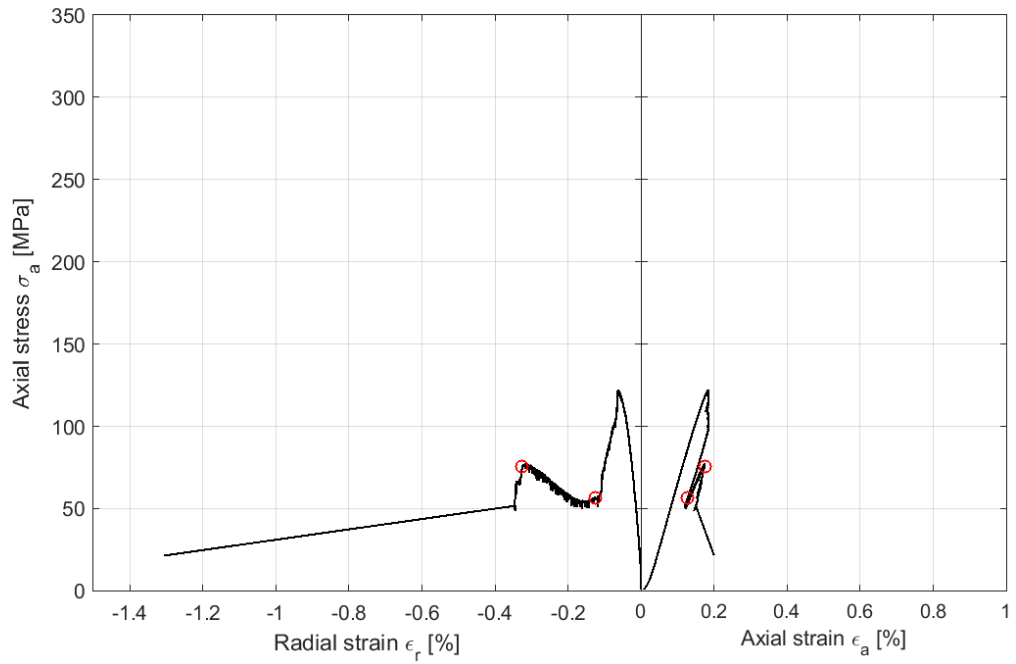
Specimen ID: KFR102A-113-08		
Before mechanical test	After mechanical test	
Diameter (mm)	**Height (mm)**	**Density (kg/m³)**	
50.2	128.9	2731	
Comments:		
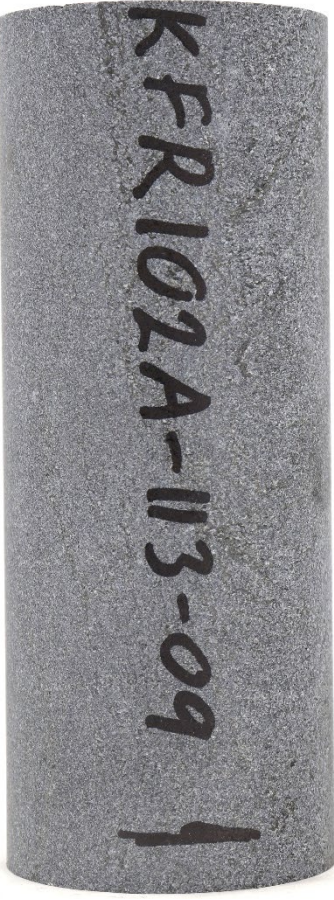
Specimen ID: KFR102A-113-08

Youngs Modulus (E):	76.4	[GPa]
Poisson Ratio (ν):	0.307	[-]
Axial peak stress (σ_c):	244.8	[MPa]
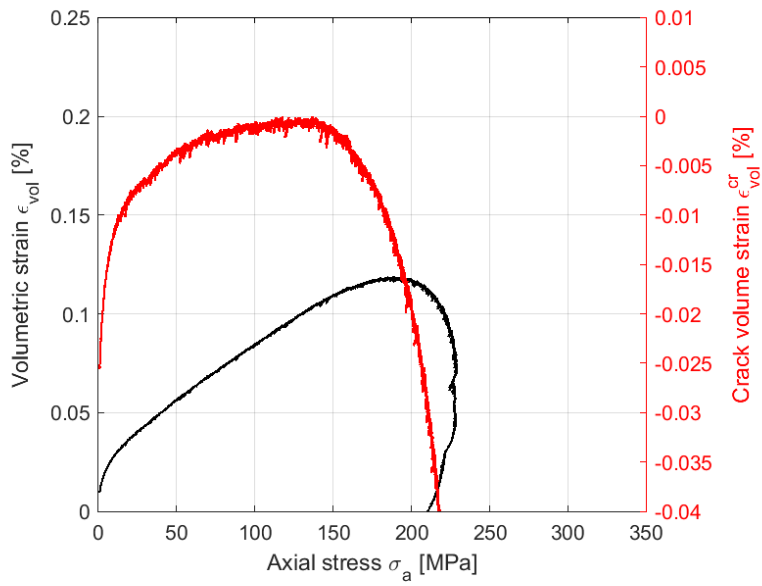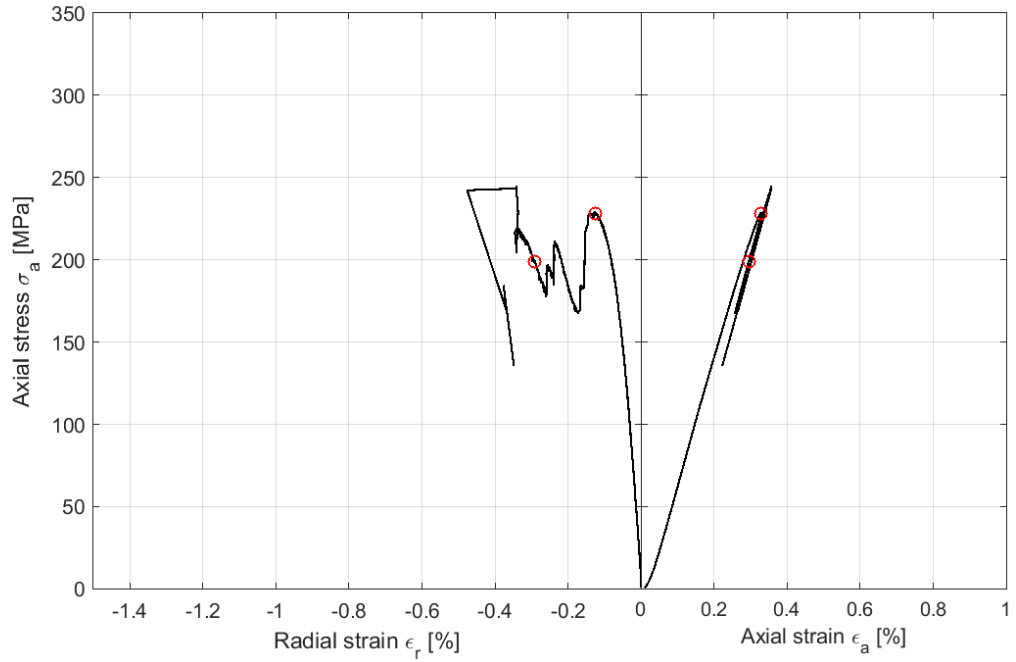
Specimen ID: KFR102A-113-09			
Before mechanical test	After mechanical test		
Diameter (mm)	Height (mm)	Density (kg/m³)	
50.2	128.0	2750	
Comments:			
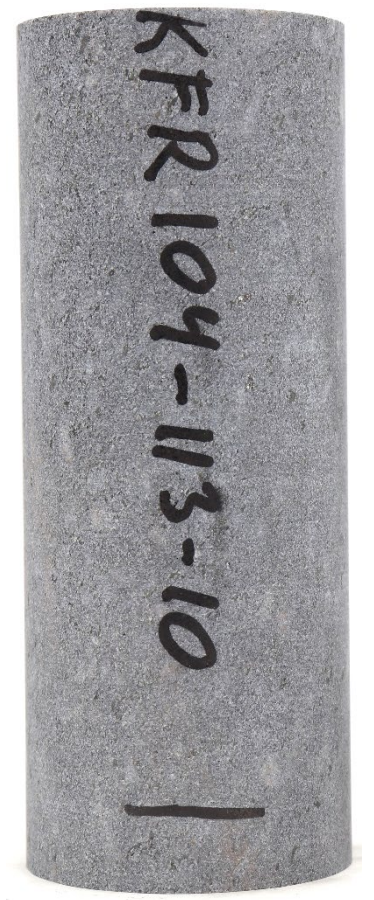
Specimen ID: KFR102A-113-09

Youngs Modulus (E):	68.2	[GPa]
Poisson Ratio (ν):	0.276	[-]
Axial peak stress (σ_c):	104.1	[MPa]

Specimen ID: KFR104-113-10			
Before mechanical test	After mechanical test		
Diameter (mm)	**Height (mm)**	**Density (kg/m³)**	
50.0	128.1	2712	
Comments:			

Specimen ID: KFR104-113-10

Youngs Modulus (E):	89.1	[GPa]
Poisson Ratio (ν):	0.313	[-]
Axial peak stress (σ_c):	283.1	[MPa]
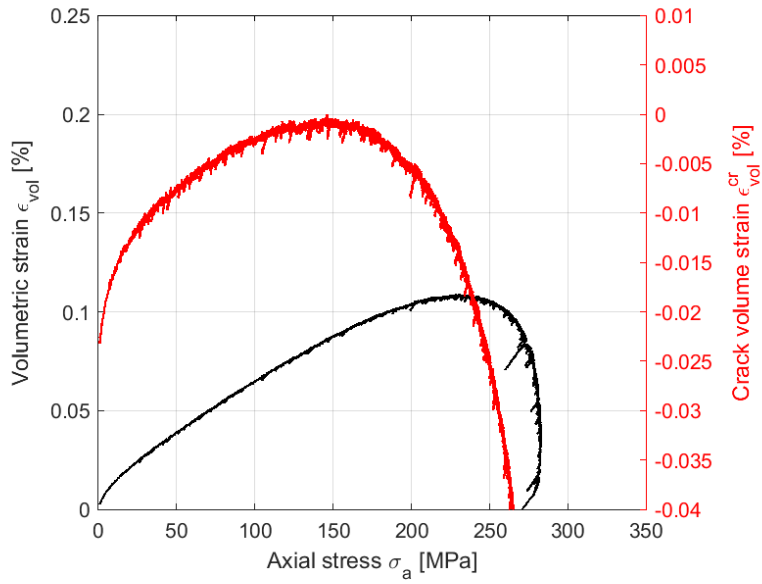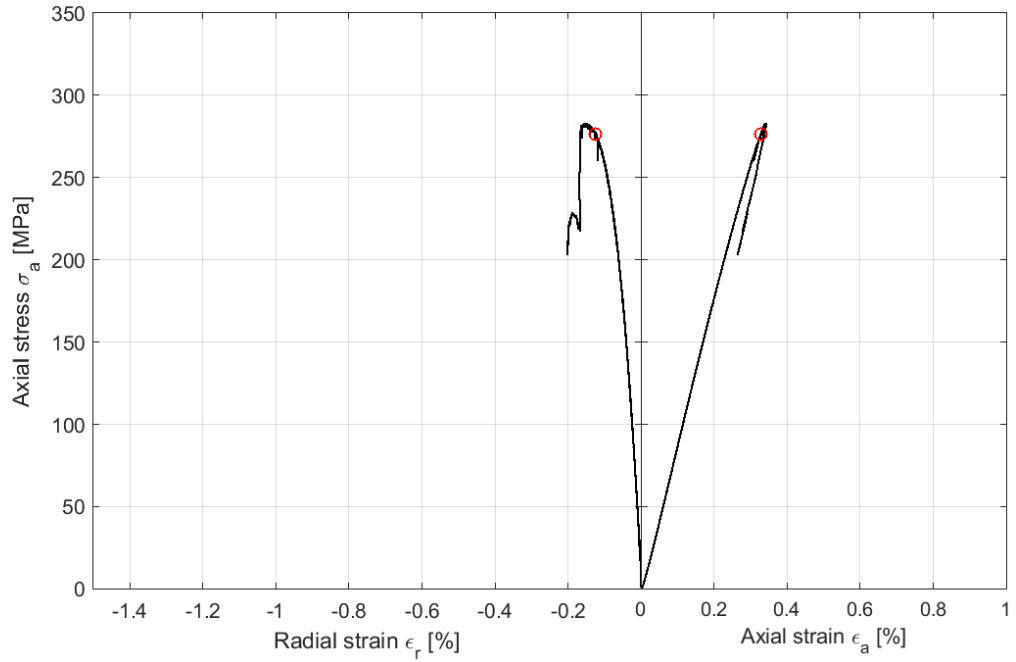
5.3.2 Results for the entire test series

A summary of the test results is shown in Table 5-2. The uniaxial compressive strength, Young's modulus and Poisson ratio as a function of the borehole length for the two rock types are shown in Figure 5.3, Figure 5.4 and Figure 5.5 respectively.

Table 5-2. Results from density measurements and uniaxial compression tests.

Identification	Density (kg/m³)	Compressive strength (MPa)	Young's modulus (GPa)	Poisson's ratio (-)
KFM01A-113-01	2959	213.1	88.6	0.386
KFM01A-113-02	3037	333.7	114.5	0.345
KFM08A-113-03	2979	289.2	101.4	0.339
KFM08A-113-04	3059	44.5	41.2	0.500 (*)
KFM08A-113-05	2900	252.9	89.3	0.384
KFM11A-113-06	2701	132.4	88.8	0.236
KFM11A-113-07	2757	122.2	77.3	0.326
KFR102A-113-08	2731	244.8	76.4	0.307
KFR102A-113-09	2750	104.1	68.2	0.276
KFR104-113-10	2712	283.1	89.1	0.313

(*) The loading curve and the value on Poisson's ratio show that there has been an inhomogeneous deformation during loading.
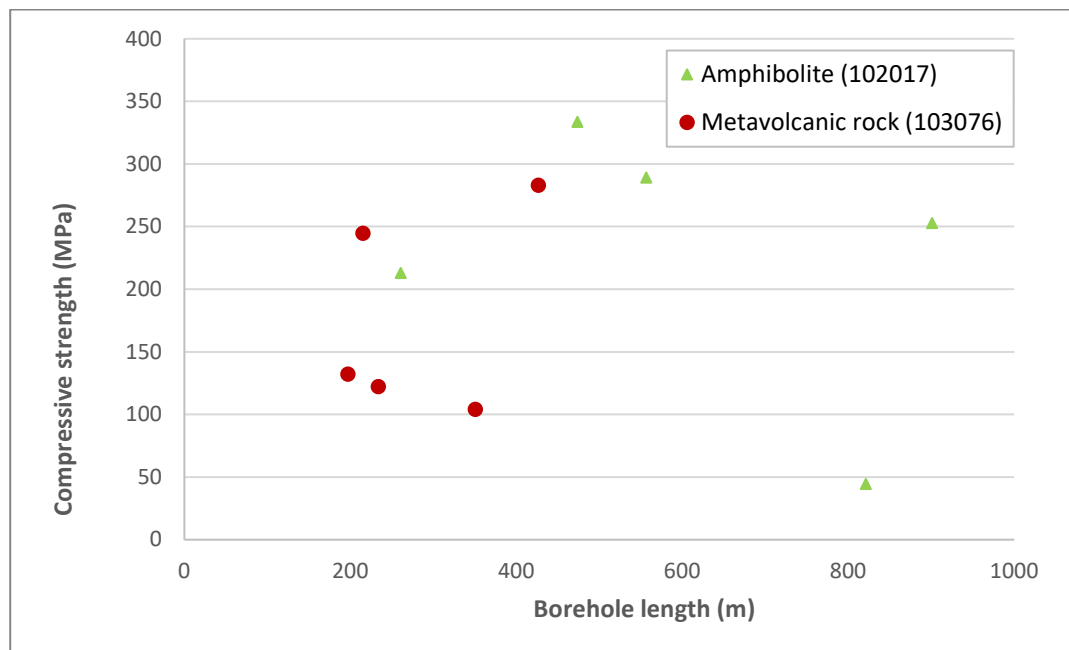
Figure 5-3. *Uniaxial compressive strength as a function of the borehole length for the two rock types.*
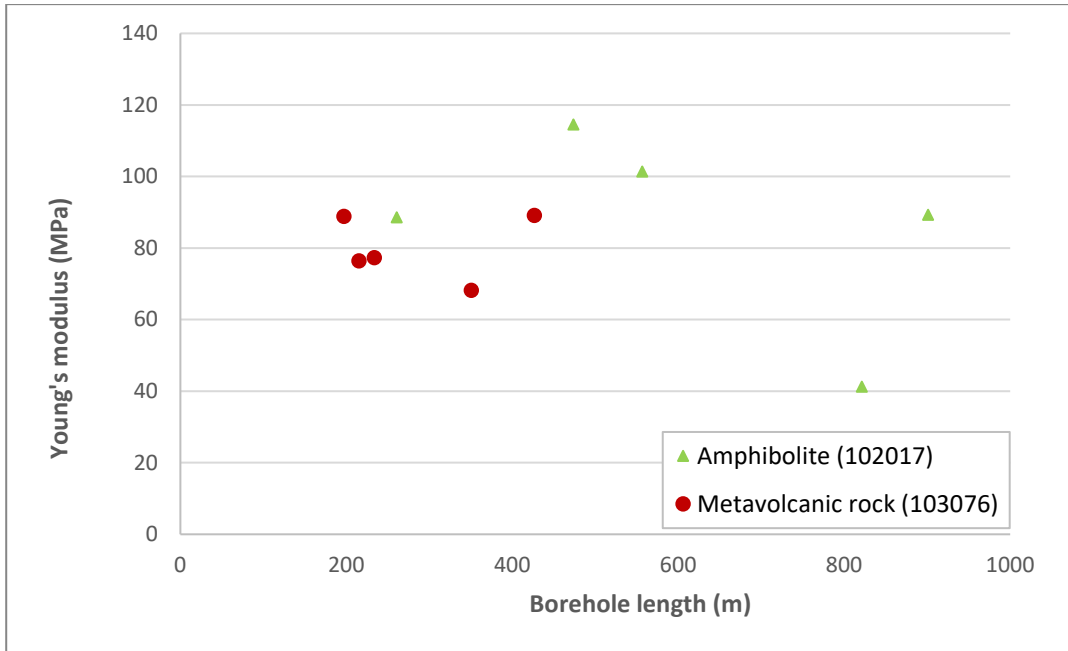
Figure 5-4. *Young's modulus as a function of the borehole length for the two rock types.*
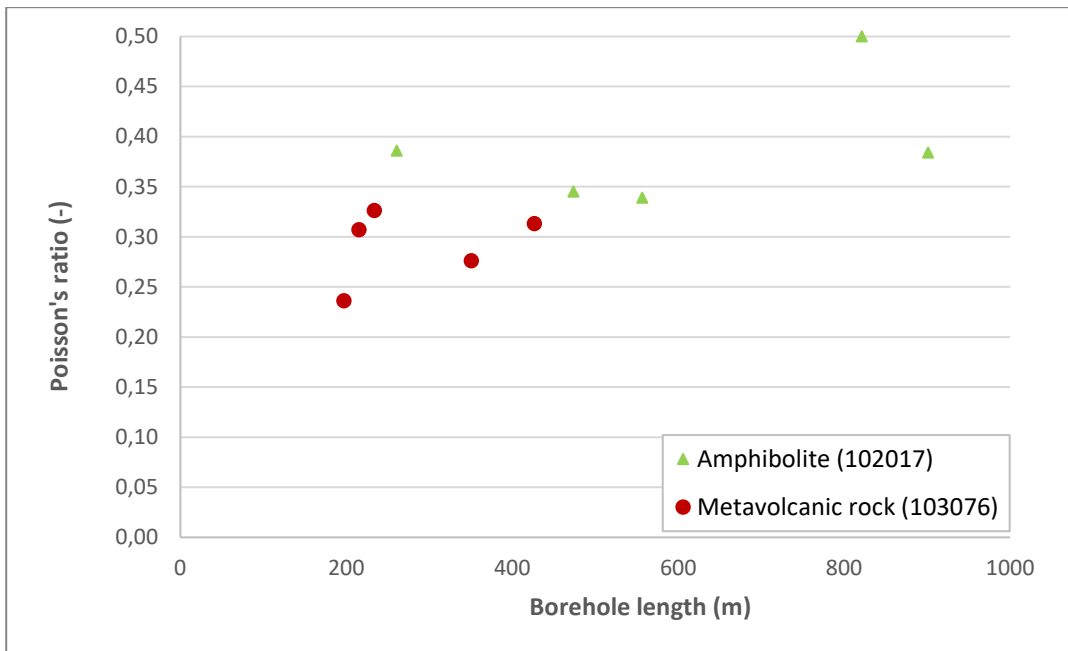
Figure 5-5. *Poisson's ratio as a function of the borehole length for the two rock types.*

References

SKB's (Svensk Kärnbränslehantering AB) publications can be found at www.skb.com/publications. SKBdoc documents will be submitted upon request to document@skb.se.

ASTM, 1996. ASTM D3967-95a, Standard test method for splitting tensile strength of intact rock core specimens. West Conshohocken, PA: ASTM International.

ASTM, 2001. ASTM 4543-01, Standard practice for preparing rock core specimens and determining dimensional and shape tolerance. West Conshohocken, PA: ASTM International.

CEN, 2008. EN 13755:2008. Natural stone test methods - Determination of water absorption at atmospheric pressure. CEN, Brussels.

Eberhardt E, Stead D, Stimpson B, Read R S, 1998. Identifying crack initiation and propagation thresholds in brittle rock. Canadian Geotechnical Journal, 35, 222–233.

Ghazvinian E, Diederichs M, Martin D, Christiansson R, Hakala M, Gorski B, Perras M, Jacobsson L, 2012. Prediction thresholds for crack initiation and propagation in crystalline rocks. ISRM Commission on Spall Prediction Report on Testing Procedures, International Society for Rock Mechanics, Portugal.

ISRM, 1979. Suggested Method for Determining Water Content, Porosity, Density, Absorption and Related Properties and Swelling and Slake-durability Index Properties. International Journal of Rock Mechanics and Mining Sciences & Geomechanics Abstracts, 16(2), 141–156.

ISRM, 1999. Draft ISRM suggested method for the complete stress-strain curve for intact rock in uniaxial compression. International Journal of Rock Mechanics and Mining Sciences, 36(3), 279–289.

Jacobsson L, Sandström J, Flansbjer M, Sjögren T, Brander L, 2016. ONKALO POSE Experiment – Laboratory Determination of Density, Porosity and Mechanical Anisotropy of Gneiss and Granite. Posiva Working Report 2016-31, Posiva OY, Finland.

Martin C D, Chandler N A, 1994. The progressive fracture of Lac du Bonnet granite. International Journal of Rock Mechanics and Mining Sciences & Geomechanics Abstracts, 31(6), 643–659.

Mathworks, 2021. MATLAB Release 9.11.0.1769968 (R2021b). Natick, MA: The MathWorks, Inc.

Stråhle A, 2001. Definition och beskrivning av parametrar för geologisk, geofysisk och bergmekanisk kartering av berg. SKB R-01-1, Svensk Kärnbränslehantering AB.

Appendix 1

The following equations describe the calculation of radial strains when using a circumferential deformation device, see Figure A1-1.

$$\varepsilon_r = \frac{\Delta C}{C_i}$$

where

$C_i = 2\pi R_i$ = initial specimen circumference

ΔC = initial specimen circumference = $\dfrac{\pi \Delta X}{\sin(\theta_i/2) + (\pi - \theta_i/2)\cos(\theta_i/2)}$

and

ΔX = change in LVDT reading = $X_i - X_f$

(X_i = initial chain gap; X_f = current chain gap)

θ_i = initial chord angle = $2\pi - \dfrac{L_c}{R_i + r}$

L_c = chain length (measured from center of one end roller to center of the other end roller)

r = roller radius

R_i = initial specimen radius
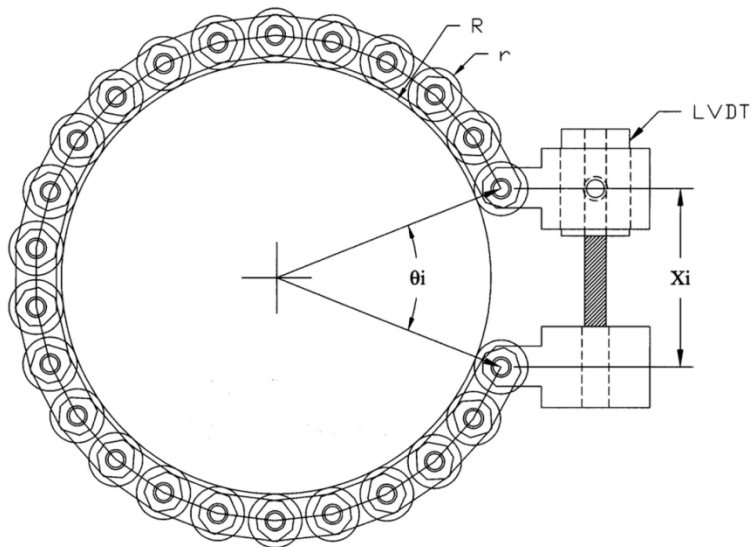
Figure A1-0-1. Chain for radial deformation measurement.

Appendix 2

This Appendix contains results showing the unprocessed data and values on the computed system stiffness K_{system} that was used for the data processing, cf. Section 4.4.2. In addition, graphs showing the volumetric strain ε_{vol} versus the axial strain ε_a and the actual radial strain rate $d\varepsilon_r/dt$ versus time are also displayed.

Specimen ID: KFM01A-113-01
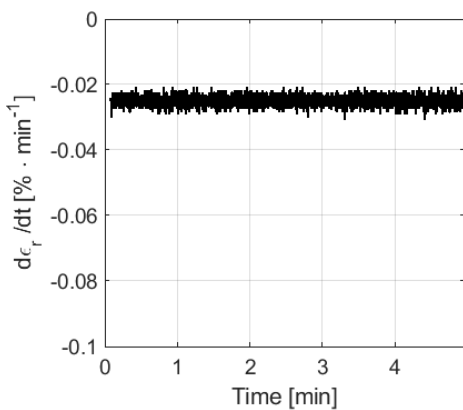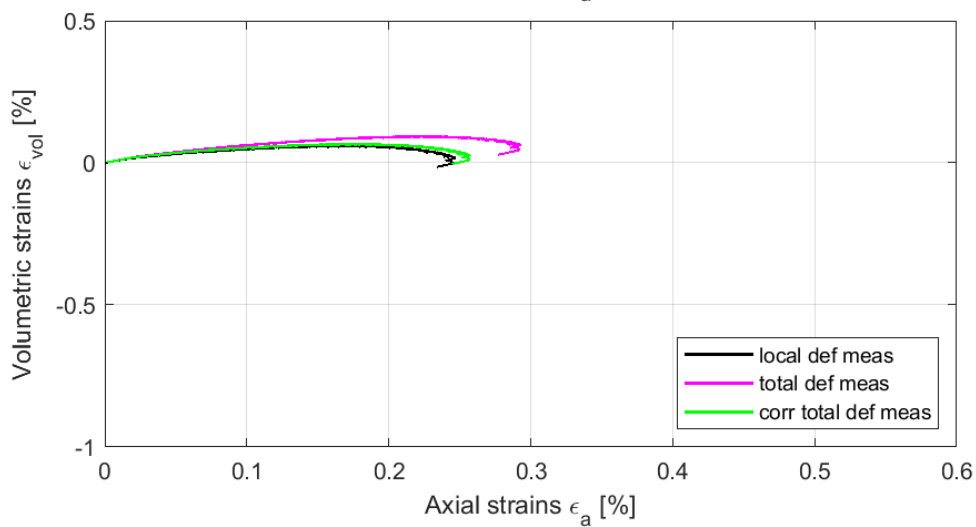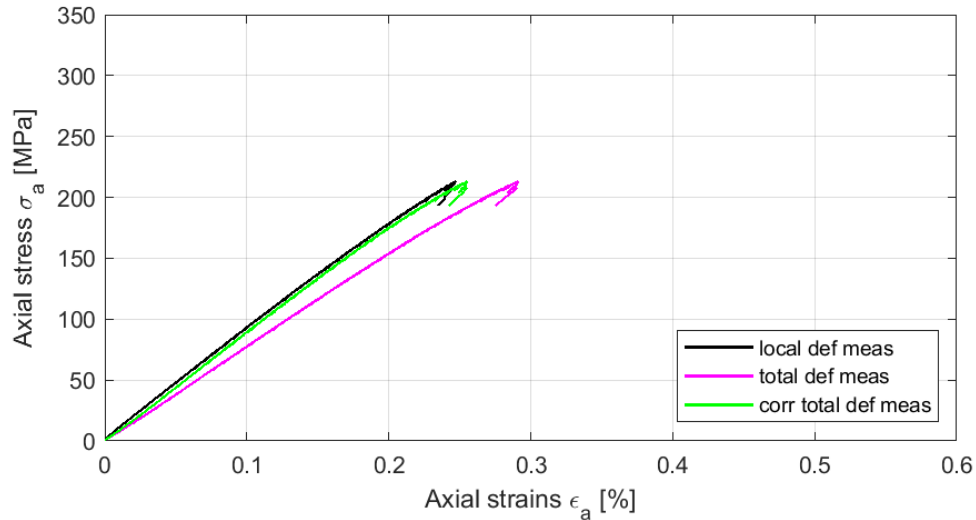
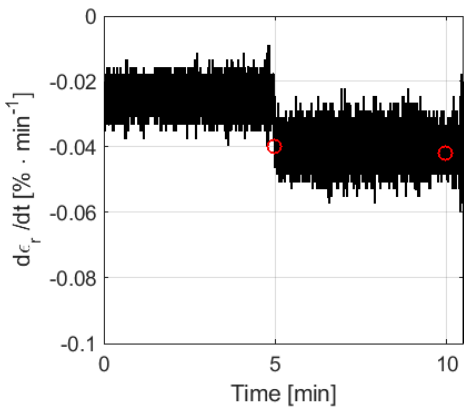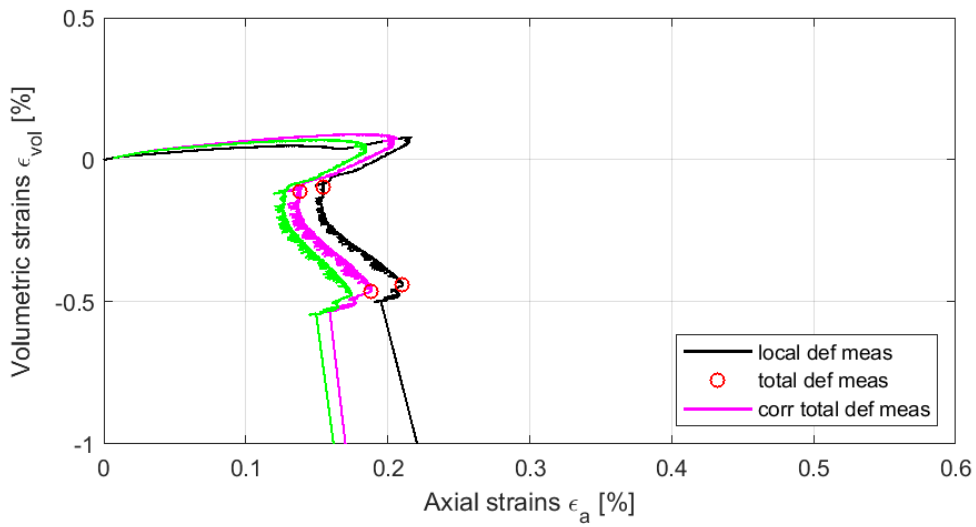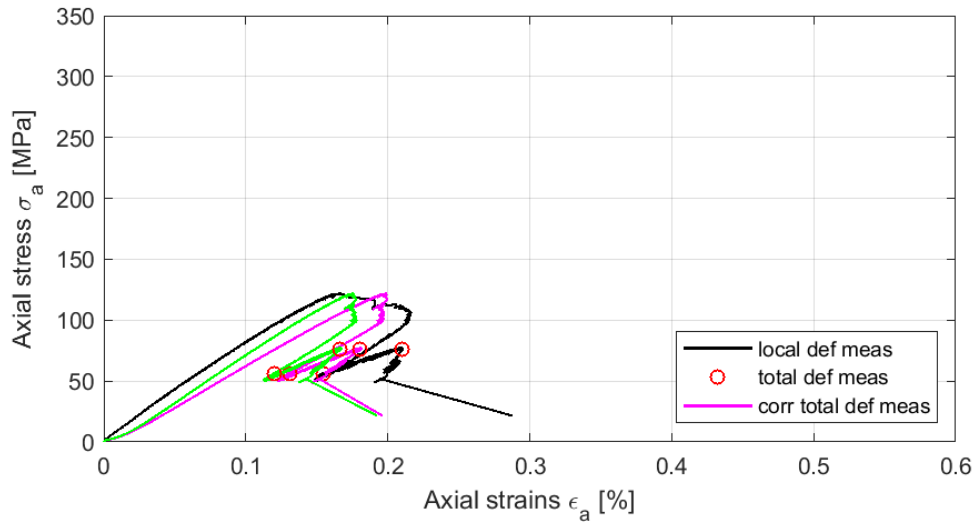Explanation to curves above:

Based on local deformation (black)

Based on total deformation (magenta)

Based on corrected deformation (green)

Calculated system stiffness:

K_{system} = 9.4 [GN/m]
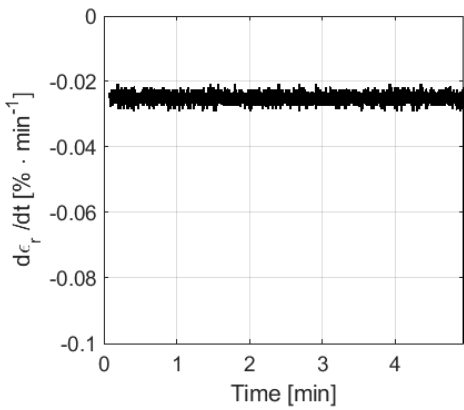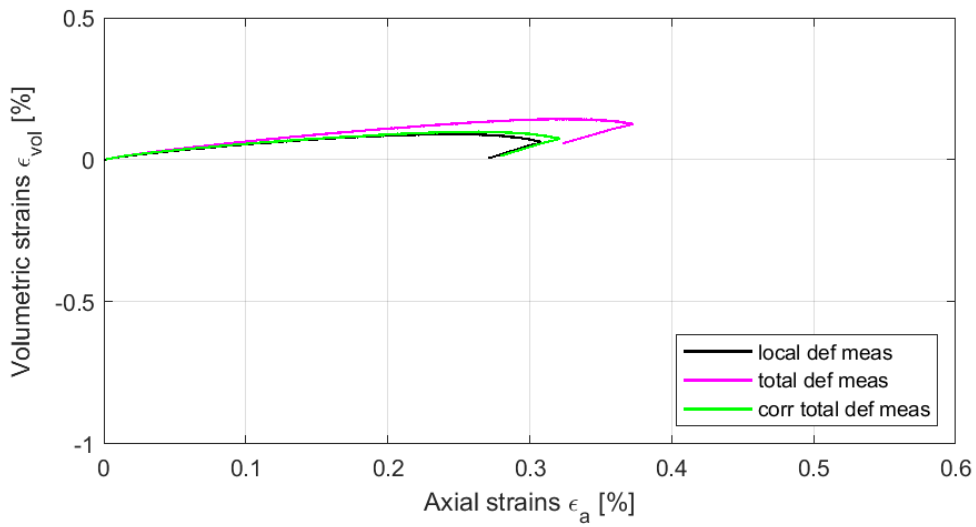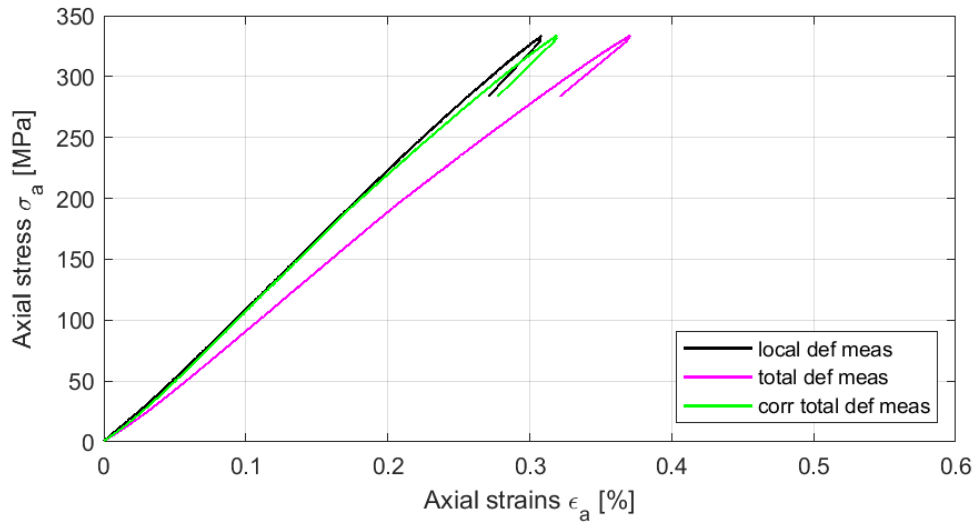
58

Specimen ID: KFM01A-113-02

Explanation to curves above:

Based on local deformation (black)

Based on total deformation (magenta)

Based on corrected deformation (green)

Calculated system stiffness:

K_{system} = 10.3 [GN/m]

Specimen ID: KFM08A-113-03
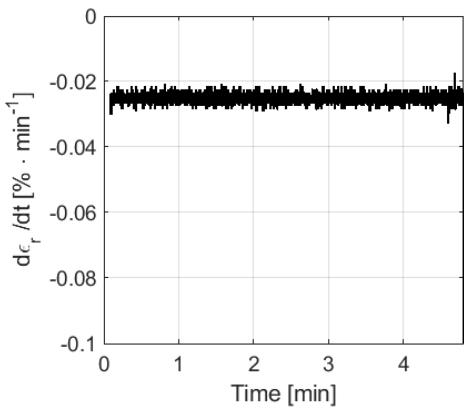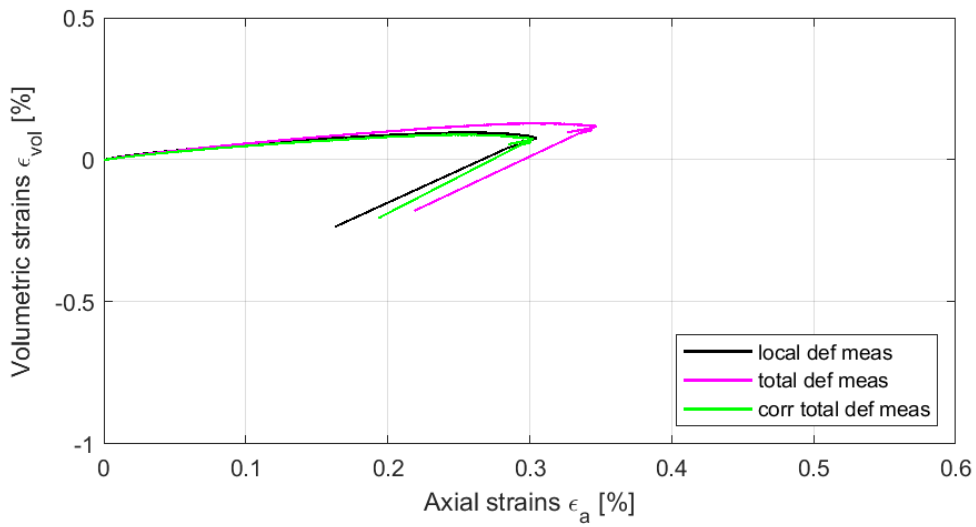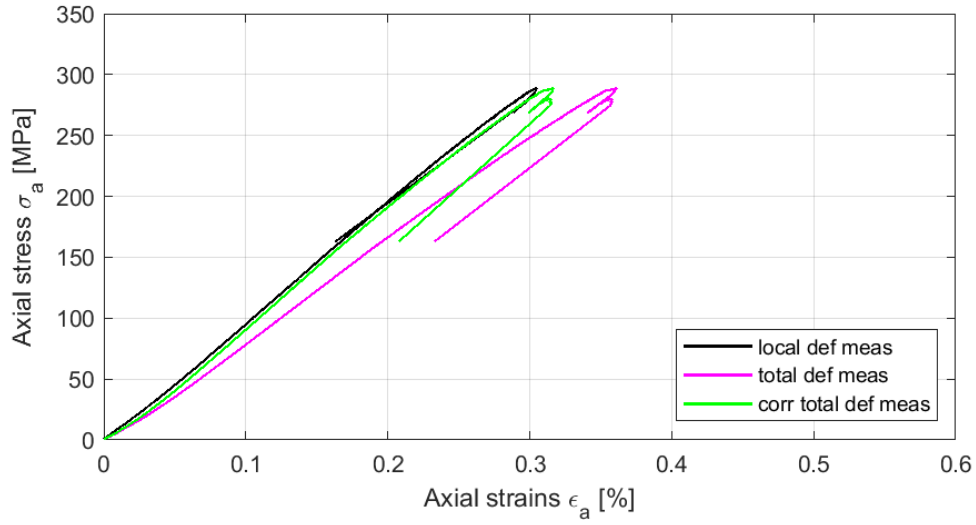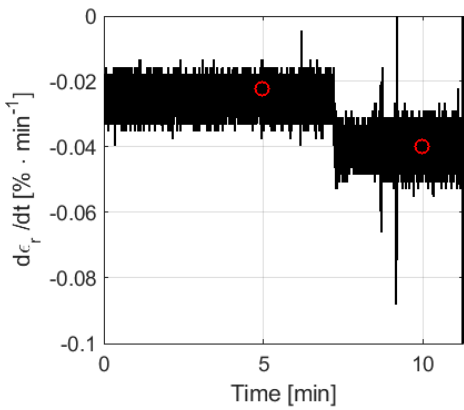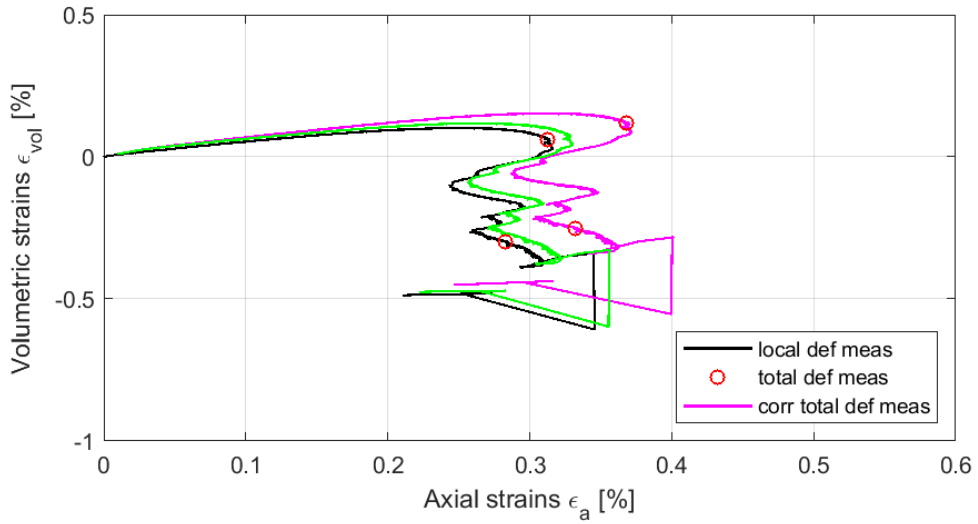

Explanation to curves above:

Based on local deformation (black)

Based on total deformation (magenta)

Based on corrected deformation (green)

Calculated system stiffness:

K_{system} = 10 [GN/m]

Specimen ID: KFM08A-113-04
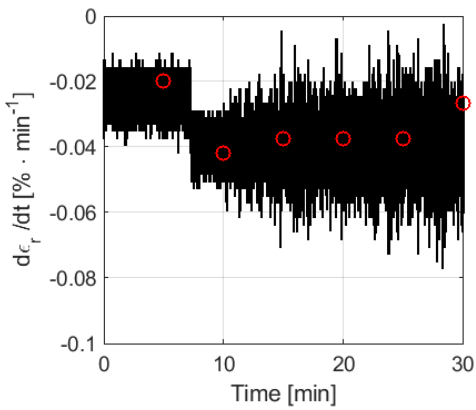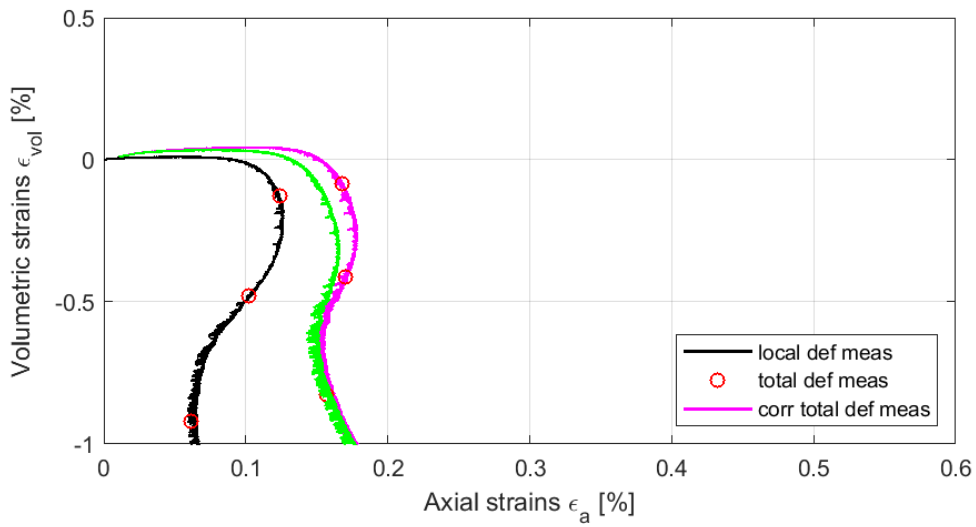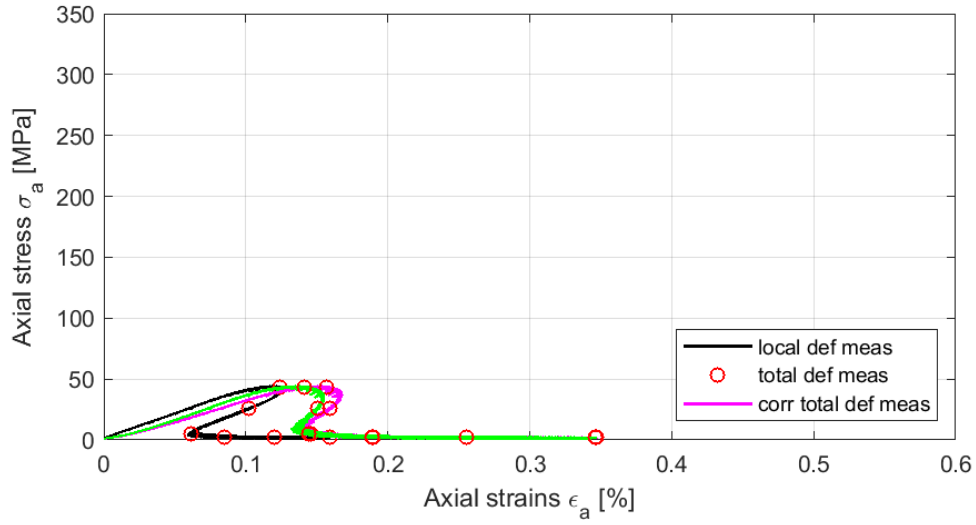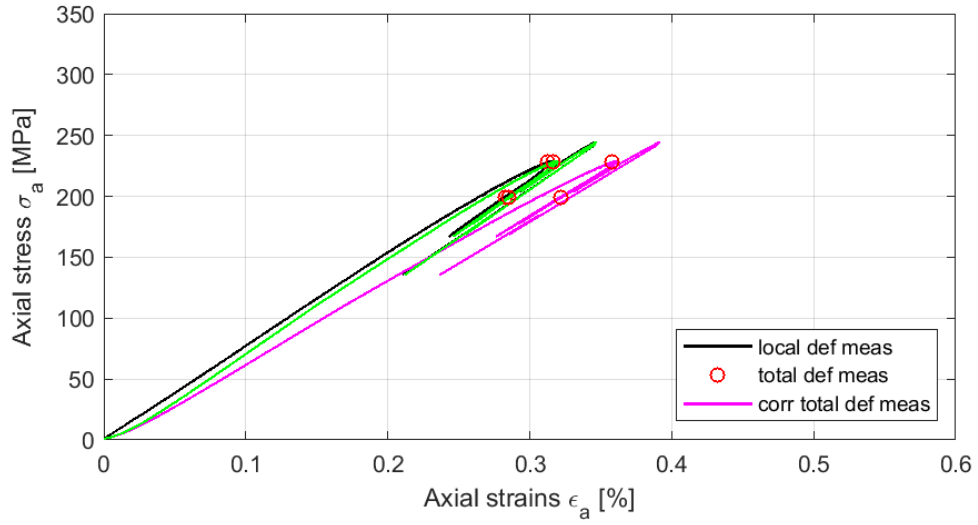

Explanation to curves above:

Based on local deformation (black)

Based on total deformation (magenta)

Based on corrected deformation (green)

Calculated system stiffness:

K_{system} = 4.4 [GN/m]

Specimen ID: KFM08A-113-05
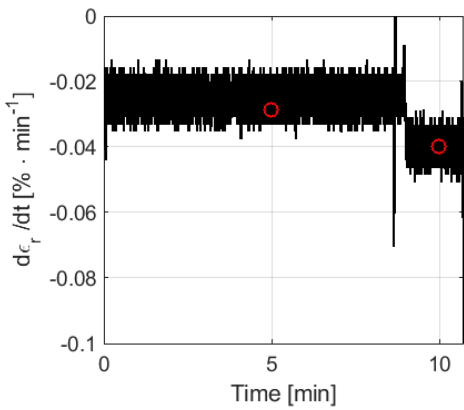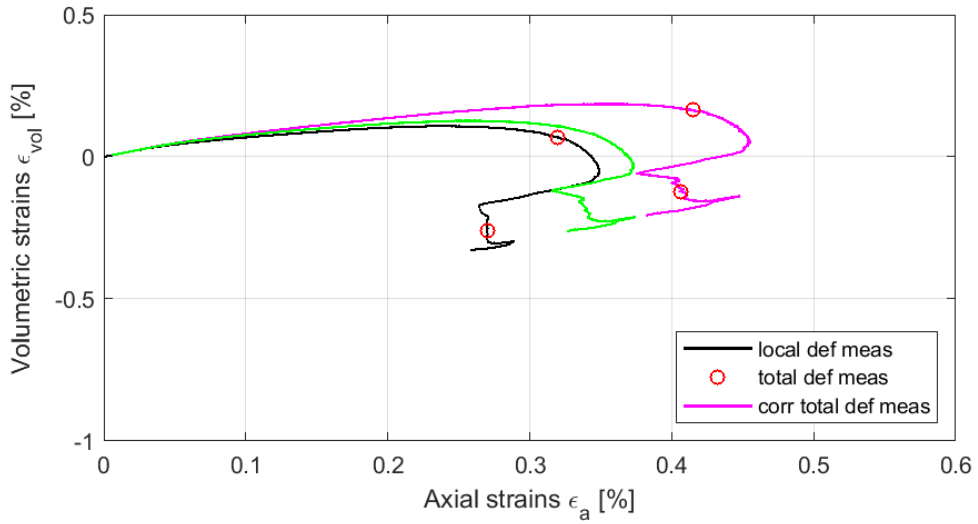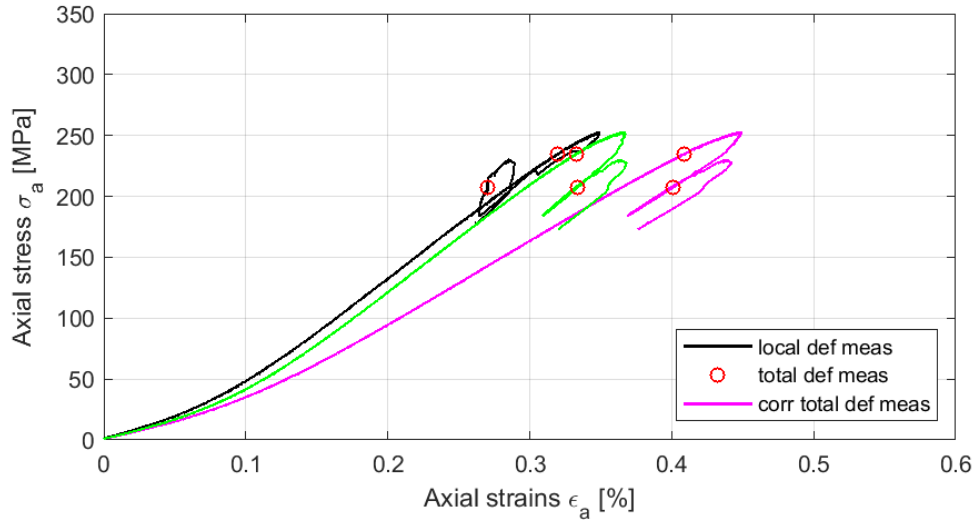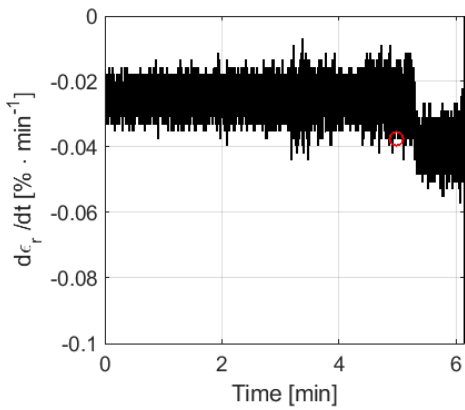

Explanation to curves above:

Based on local deformation (black)

Based on total deformation (magenta)

Based on corrected deformation (green)

Calculated system stiffness:

K_{system} = 4.8 [GN/m]

Specimen ID: KFM11A-113-06
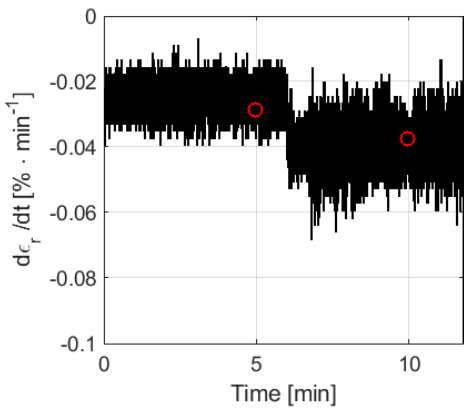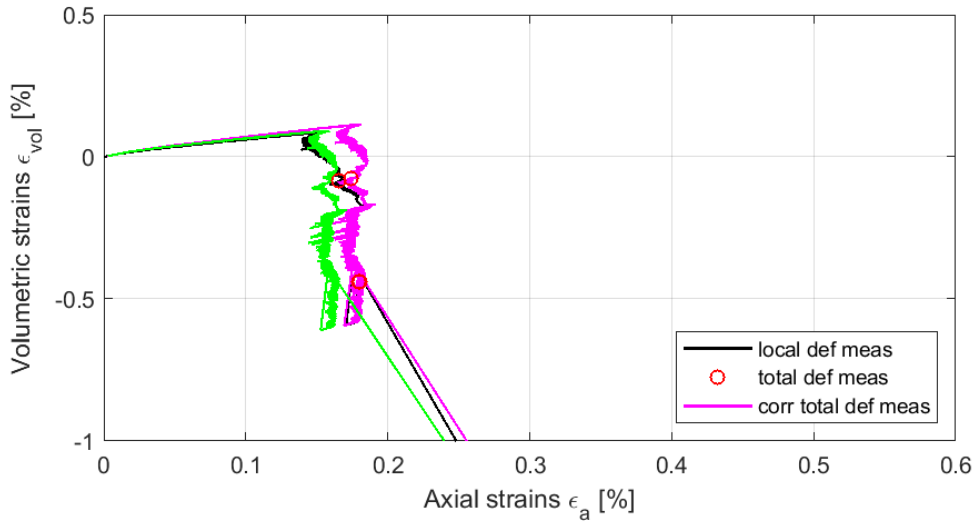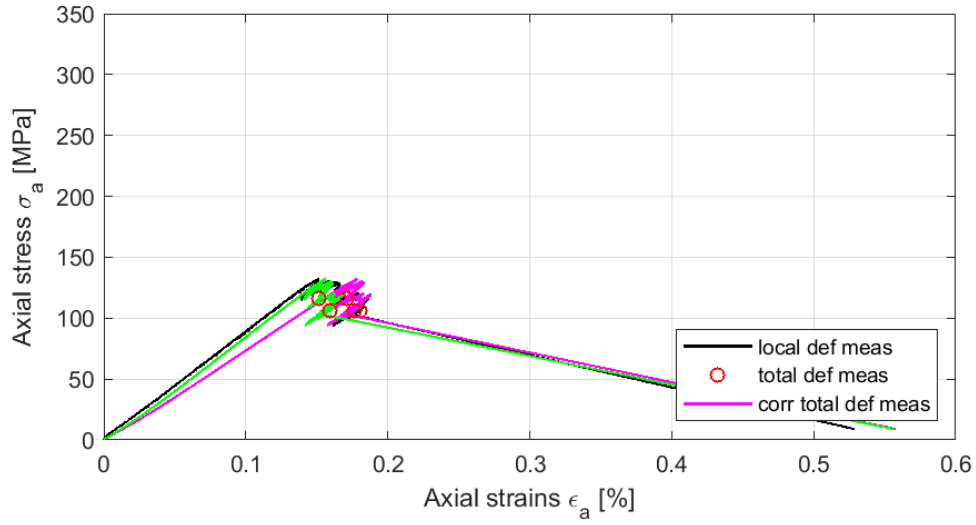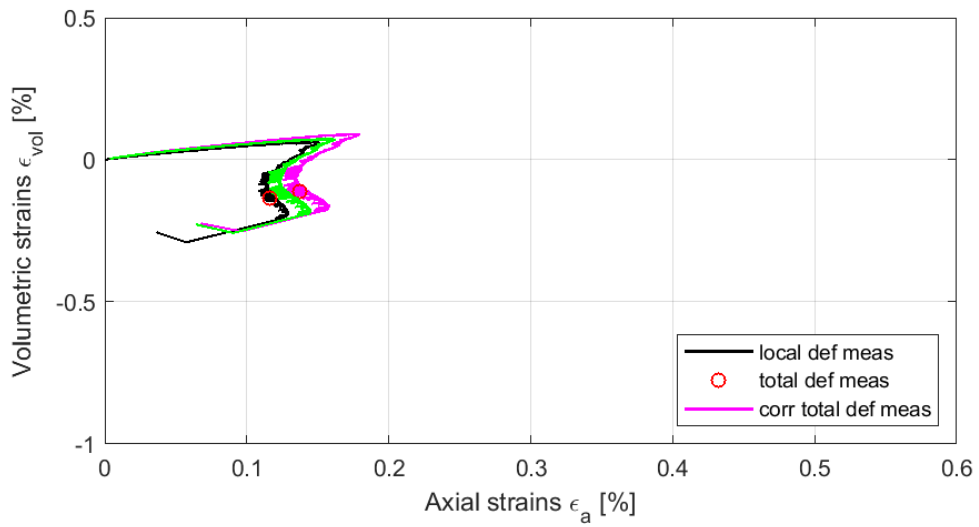

Explanation to curves above:

Based on local deformation (black)

Based on total deformation (magenta)

Based on corrected deformation (green)

Calculated system stiffness:

K_{system} = 9.3 [GN/m]

Specimen ID: KFM11A-113-07

Explanation to curves above:

Based on local deformation (black)

Based on total deformation (magenta)

Based on corrected deformation (green)

Calculated system stiffness:

K_{system} = 8.3 [GN/m]

Specimen ID: KFR102A-113-08

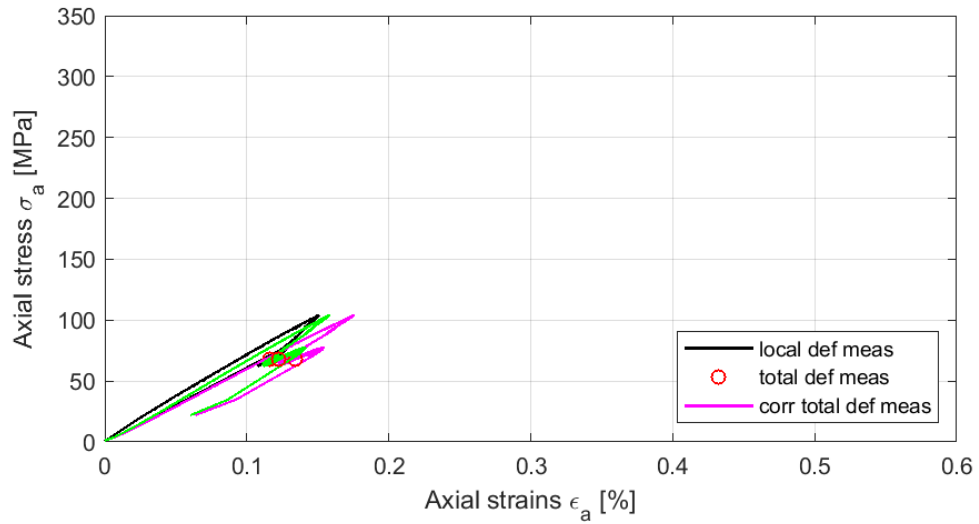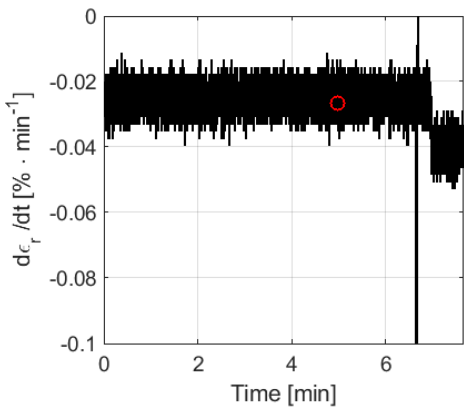Explanation to curves above:

Based on local deformation (black)

Based on total deformation (magenta)

Based on corrected deformation (green)

Calculated system stiffness:

K_{system} = 8.4 [GN/m]

Specimen ID: KFR102A-113-09

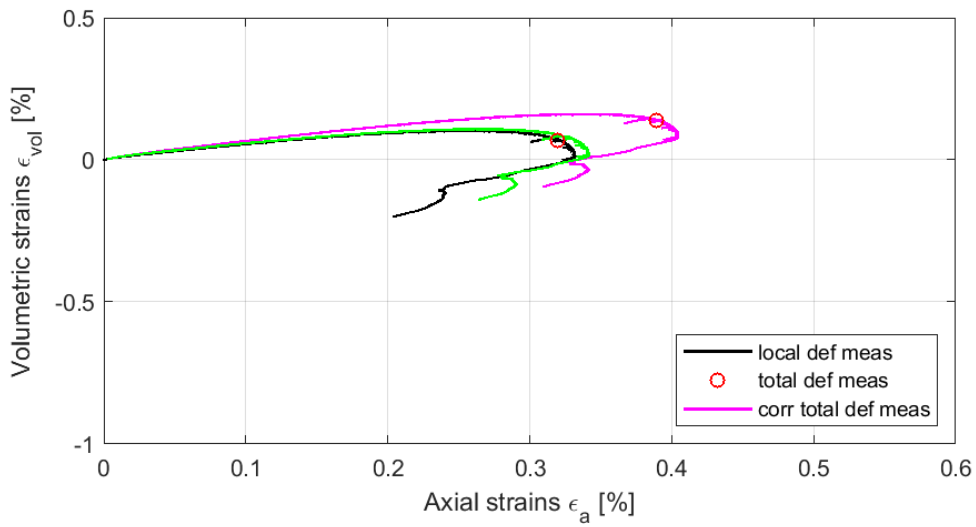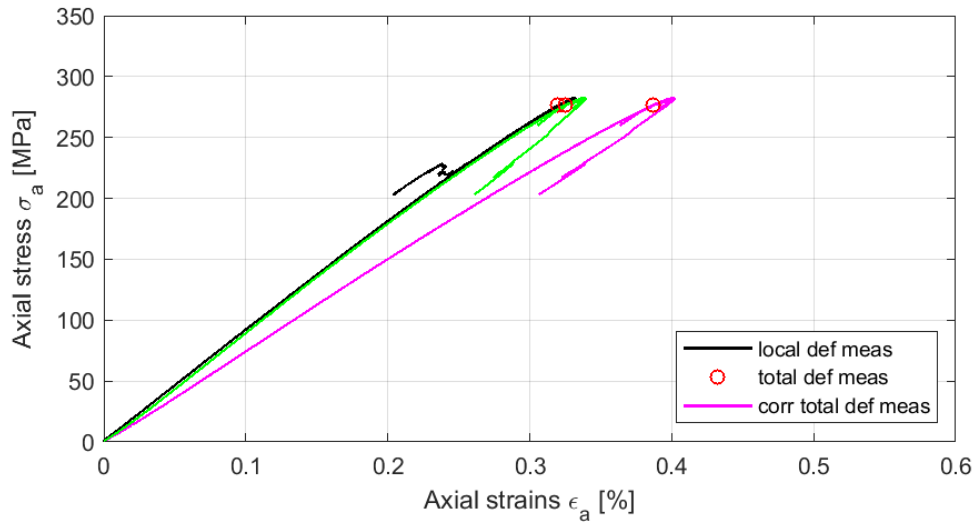Explanation to curves above:

Based on local deformation (black)

Based on total deformation (magenta)

Based on corrected deformation (green)

Calculated system stiffness:

K_{system} = 9.2 [GN/m]

Specimen ID: KFR104-113-10

Explanation to curves above:

Based on local deformation (black)

Based on total deformation (magenta)

Based on corrected deformation (green)

Calculated system stiffness:

K_{system} = 6.9 [GN/m]